Internal Report
DESY F41-77/04
May 1977

Photoemission from Semiconductor Surfaces

by

W. Gudat and D. E. Eastman

PHOTOEMISSION FROM SEMICONDUCTOR SURFACES

W. Gudat[+] and D.E. Eastman[++]

[+] Deutsches Elektronen-Synchrotron DESY, Notkestraße 85, 2 Hamburg 52

[++]IBM T.J. Watson Research Center, Yorktown Heights, N.Y. 10598

Chapter 11

of

"Photoemission from Surfaces"

Edited by

B. Feuerbacher, B. Fitton, and R.F. Willis

11. PHOTOEMISSION FROM SEMICONDUCTOR SURFACES

W. Gudat and D.E. Eastman

Contents

11. PHOTOEMISSION FROM SEMICONDUCTOR SURFACES

The existence and importance of surface states on semiconductor surfaces has long been recognized, e.g. see the early work of Bardeen [1], which considered the rectifying properties of semiconductor - to - metal point contacts. In the first systematic photoelectric studies on semiconductor surface states by Allen and Gobeli [2-4], the existence of two types of surface states - empty and occupied states - was demonstrated as well as the crucial importance of the surface geometry on the surface electronic properties. Subsequently surface states have been studied with a variety of experimental techniques, with every technique having its special advantages[5].

Basic information on surface geometries has been obtained with low energy electron diffraction (LEED)[6]. With optical absorption[7] and electron energy loss experiments[8,9] transition energies and the coupling effects between initial occupied and final empty states are established. Photoconductivity measurements[10] probe the distribution of empty surface states, whereas field emission experiments[11] and ion neutralization spectroscopy (INS)[12] allow the determination of occupied surface state levels. INS gives access to a wide energy range of the valence band in contrast to field emission which probes the energy range of the thermal gap. Photoelectron energy distribution measurements - including the various photoyield spectroscopy techniques recently developed - allow a straight forward determination of occupied and empty surface states, respectively. In particular, the new technique of angular resolved photoemssion studies is extremely useful since it gives the possibility of detecting surface states in the presence of degenerate bulk states and of directly measuring their momentum dispersion.

In this chapter we primarily discuss some of the more recent results of photoemission experiments on the best understood semiconductor surfaces in order to show the important effects and the present state of theoretical understanding. Before proceeding we discuss briefly some aspects of the novel photoemission techniques of angular resolved and yield spectroscopy experiments. For more detailed descriptions the reader is referred to two chapters of this book by Smith and Larsen and by Kunz, respectively.

We summarize some basic ideas and theoretical results in the beginning of Section 11.2 and continue a discussion on intrinsic surface properties of silicon and germanium. In Section 11.3 a discussion of surface states on compound semiconductors is presented. Here we will mainly describe the results on GaAs, which is the most thoroughly studied III-V semiconductor. A few examples of the many extrinsic effects such as cleavage steps and absorbate induced changes in the surface electronic properties are given in Section 11.4.

11.1 Experimental Techniques

A variety of complemental experimental methods are available for the study of surface electronic properties, and it is often desirable and/or necessary to incorporate more than one of the methods in an experiment. This is most easily accomplished with photoemission techniques, if particularly synchrotron radiation is available as a light source (see chapter 15). The intense, polarized, and continously tunable light allows conventional photoelectron energy distributions (PED), both angle-integrated and angle-resolved, as well as various yieldtype spectroscopy measurements.

With photoelectron energy distributions essentially occupied electronic states are probed. This is discussed at length in chapters 1 and 15 of this book. In contrast to the standard photoemission technique, in angular resolved photoemission experiments the trajectory of the photoemitted free electron to the energy analyser is accurately

measured as well as the kinetic energy. This determines the wavevector of the free photoelectron. In order to relate the observed photoelectron to its initial state and final state within the solid, it is assumed that the component to its momentum parallel to the surface $\underset{\sim}{k}_{//}$ is conserved to within a reciprocal lattice vector during the photoemission process. Thus within the direct transition model, $\underset{\sim}{k}_{//}$ of the initial electronic state is determined directly from experiment by the simple relation[13,14] (within a reciprocal lattice vector)

$$\underset{\sim}{k}_{//} = (2mE_k/\hbar^2)^{1/2} \sin\Theta$$

where E_k is the measured kinetic energy given by $E_k = \hbar\omega - \phi_\omega + E_i$ ($\hbar\omega$ = photon energy, ϕ_ω = work function, E_i = initial state energy and Θ is the polar angle measured between the surface normal and the electrons trajectory).

In the case of occupied surface states (or more generally of 2-dimensional systems) one can directly obtain from the experiment the 2-dimensional bandstructure $E(\underset{\sim}{k}_{//})$. This will be discussed later. The determination of the perpendicular component ($k_\perp$) of $\underset{\sim}{k}$ is a more involved task since it is not strictly conserved, and the full bandstructure $E(\underset{\sim}{k})$ is not readily obtained. Also, there is significant momentum broadening of $k_\perp$ due to electron-electron interactions, which has been discussed by Feibelman and Eastman[15]. One of the advantages of angle-resolved measurements is the fact that occupied surface states can be detected with far greater sensitivity than with conventional angle integrated measurements; namely by measuring only those electrons having an energy with parallel momentum k that matches that of a surface state, significant emission from the surface state can occur while the bulk emission is strongly suppressed.

With photoemission yield spectroscopies[16-18] empty surface states can be studied. Our definition of yield spectroscopy includes all techniques in which the photon energy is scanned either with the electron energy being fixed or varied. We now briefly describe the physical processes underlying these yield spectroscopy techniques as well as the operational procedures used to implement them. In connection with synchrotron radiation light sources,[19] yield spectroscopy techniques are usually used to probe transitions between core levels and empty states. Since core levels have negligible dispersion in wavevector space, essentially the unoccupied conduction band and surface state band density of states is measured. However, the early yield spectroscopy experiments on surface states by Allen and Gobeli[2-4] and their high sensitivity counterparts described by Sebenne and coworkers[20] mainly probe transitions between occupied surface and bulk states to states just at or above the vacuum level.

In the former experiments, one measures electrons that are indirectly generated by optical transitions from a core level to empty surface states[18] and/or conduction band states[16]. The sensitivity for strongly observing surface states occurs because only optical excitations within an effective electron escape depth (roughly 5-30 Å) can contribute to the measured photocurrent. The heuristic explanation for observing empty states is as follows:[16] After the primary photoabsorption of a photon, the excited core state becomes deexcited by one or more of the following processes:

i) Auger transitions,

ii) direct recombination processes of excitons involing the valence bands, and

iii) direct recombination of surface excitations, etc.

The resulting "fast" electrons undergo inelastic electron-electron scattering and thereby generate secondary electrons. Thus, if the optical excitation and core level Auger de-excitation and recombination pro-

cesses are uncoupled, yield spectroscopy measurements of either these secondary electrons (the partial yield spectrum), the "fast" electrons (the constant initial state spectrum), or the total number of emitted electrons (total yield spectrum), show the core level-to-surface state excitation spectrum.

With partial yield spectroscopy one measures the partial yield of electrons $N(\hbar\omega,E)$ in an electron energy window ΔE at a fixed final state energy E as a function of photon energy $\hbar\omega$. The final state energy is usually choosen to be < 5 eV so that only secondary electrons are measured; this avoids any $\hbar\omega$-dependent contribution due to primary valence electron excitations. An enhanced surface state to background ratio results, if direct Auger electrons are sampled rather than secondary electrons. However, an $\hbar\omega$-dependent spectral contribution due to primary valence electrons also occurs in this case that can contain significant structures. Although the technique of constant final state (CFS) spectroscopy is operationally the same as that of partial yield spectroscopy (PYS)) its application has been slightly different. CFS spectra have been measured at relatively high kinetic energies ($E_k > 5$ eV) in order to study initial state effects and excitonic effects[17,21].

The constant initial state (CIS) spectroscopic technique[17] consists of measuring the $\hbar\omega$-dependent partial yield of electrons $N(\hbar\omega, E_i)$ in an energy window ΔE at a fixed initial state energy $E_i = E - \hbar\omega$. This is accomplished by synchronously scanning both the optical monochromator and the electron energy analyzer with equal energy increments ΔE so that $\hbar\omega$-E is kept constant. Core level-toempty surface state transitions can be enhanced by selecting an appropriate E_i which corresponds to both a minimum in the valence band emission as well as a final energy E having intense "fast" Auger electron emission.

The total yield spectrum corresponds to measuring all emitted electrons as a function of photon energy $\hbar\omega$. This spectrum contains contributions of many kinds of electrons, primary electron emission, Auger electron emission, direct recombination emission plus secondary electron emission due to both primary and Auger electrons. Near the fundamental threshold fewer processes contribute to the total yield spectrum, and it can be used to measure photothresholds, surface states in the gap, etc.[2-4,20].

II.2 Intrinsic Surface States on Group IV Semiconductors

From low energy electron diffraction (LEED) measurements[6,22] it is known that the clean surface of many semiconductors including the group IV element semiconductors, the III-V compounds and, to a lesser extent, the II-VI compounds have atomic arrangements which are different from the atomic arrangement for the ideal truncated lattice. These modifications in surface atom positions i.e. relaxation and reconstruction, are generally not accurately known, but it is known that they strongly affect the surface electronic energy levels and surface physical properties. The Si (111) surface, which exhibits several reconstructed phases - 2x1, 7x7, 1x1 - has been the most extensively studied semiconductor surface. We describe its surface geometry together with selected experimental and theoretical studies as a prototype semiconductor surface. However, as will become evident, there are still many problems and uncertainties even for Si (111), e.g. the reconstruction geometry, which is not accurately known.

II.2.1 Surface Geometry and Electronic Structure

The (111) plane of Si is the natural cleavage plane of the group IV semiconductors having the diamond structure and thus is the most easily prepared clean surface plane. LEED studies have shown that cleaved Si (111) forms a reconstructed metastable 2x1 surface at a temperature $T \sim 25^{\circ}$ C.[10,22,23] Several phases occur at higher temperatures - an intermediate 1x1 structure, a stable 7x7 structure ($T \gtrsim 425^{\circ}$ C) and a higher temperature ($\sim 850^{\circ}$ C) 1x1 structure, which can be stabilized at room temperature with adsorbed atoms[24] or by quenching[25] as recently demonstrated.

The surface geometry and the surface Brillouin zone of the Si (111) surface are described in Fig. II.1 for the "ideal" Si (111) surface (in which the surface atoms have the same relative positions as in the bulk) and for the

reconstructed Si (111)-2x1 surface. For the latter we show a model due to Haneman[26] which is widely used and appears to best describe its surface properties. For the "ideal" surface (which does not exist), the surface atoms have broken bonds (i.e., dangling bonds) due to missing neighbours in the <111> direction (Fig. II.1). These broken bonds result in "dangling band" (DB) surface states that contain one electron, i.e. are half-filled. For the Haneman model[26] of the 2x1 surface, a "buckled" surface is obtained by a periodical raising and lowering of alternative rows of surface atoms, with the second layer atoms being shifted laterally (indicated by arrows in Fig. II.1) so as to approximately maintain the bond lengths of the three back bonds of the surface atoms. This reconstruction causes the dangling bonds of the surface atoms to partially dehybridize from bulk sp^3 into more s-like (buckled outwards) and p_z-like (buckled inwards). Slight modifications of this buckled surface reconstruction model have been used by several authors[27-30] to calculate the surface electronic structure. To date, there has been no accurate quantitative LEED analysis which unequivocably determined the atomic geometry of the Si (111)-2x1 surface. A different mechanism has been suggested by Tosatti and coworkers[31,32] involving a displacement and a tilting of the dangling bonds towards each other to yield a pairing of surface atoms.

The surface unit cell of Si (111)-2x1 is given in Fig. II.1d; it is twice as large as the bulk unit cell in the $(\bar{1}12)$ direction. The surface Brillouin zone (BZ) changes from a hexagon for the (1x1) structure into a rectangle having half the area of the original zone for the 2x1 structure. There are 2 different atoms in the 2x1 unit cell which cause the band of DB surface states to split into two along the edge of the new BZ, as we shall se below.

Before proceeding to describe selected experimental result, it is useful to briefly describe selected theoretical studies of the Si (111) surface, which indicate the nature and types of surface states that can occur. During the past few years, major theoretical progress in semiconductor surface state calculations has occured. Reviews of earlier and recent work have been given by Davisson and Levine[33], Garcia-Moliner and Flores[34], Appelbaum and Hamann[35], and Forstmann (chapter 8, this book).

A major advancement in semiconductor surface calculations was the physically realistic calculation for both the ideal and relaxed Si (111) surface by Appelbaum and Hamann[36]. They found a dangling bond surface state near the band gap for both geometries. While such states had been previously predicted, they also found new surface states that depended on the atomic arrangement. Namely, for a geometry with the surface atoms relaxed inwards, they found additional bands of surface states near the bottom of the lowest valence band and within the p-like region of the bulk band structure. The more recent work by Pandey and Phillips[28,29,37] and Schlüter et al.[38-40] confirm these spectral findings. These surface state features are shown for a relaxed Si (111)-1x1 surface (0.33 Å contraction)[29] in Fig. 11.2, which compares the local density of states (LDOS) of the first (outer) layer and fourth layer with that of the bulk. (The LDOS for a layer is defined as the energy distribution of electron states localized on atoms in that layer.) Features near 0 eV (dangling bond), -4 eV and -11 eV (saddle point peaks in back-bond-surface bands) corresponds to those discussed by Appelbaum and Hamann.[36]

Several of the more realistic calculations for the Si (111)-2x1 surface are those of Schlüter et al.[38-40], Pandey and Phillips[28,29] and Ciraci and Batra[41,42] which have all assumed variations of the Haneman model.[26]

Upon reconstructing into the 2x1 structure, the DB state (see Fig. 11.2) splits into two, with the states associated with the upwards expanded atoms dropping in energy and those associated with the contracted atoms forming the upper branch. A LDOS calculated by Schlüter et al.[39,40] for these states for Si (111)-2x1 is shown in Fig. 11.3. Here the Haneman[26] model was used with alternating rows of atoms being raised and lowered by 0.18 Å and 0.11 Å, respectively. In addition to the dangling bond states, lower-lying surface states associated with transverse backbonds and longitudinal backbonds were found.[38-40] The computational results of Appelbaum and Hamann[27,36], Schlüter et al.[38-40] and Pandey and Phillips[28,29,37] appear consistent with each other; namely, existing differences in the number of surface states and in surface state energies (to within ~0.3 eV) in the various model calculations appear to be due to the various assumed geometries.

11.3.2 Intrinsic Surface States on Silicon

In their pioneering work on clean silicon surfaces, Allen and Gobeli[2,3] determined the existence of intrinsic occupied and empty surface states on Si (111)-2x1 and Si (111)-1x1. They used extensive band bending measurements to determine the Fermi level E_F at the surface (E_F-E_V, where E_V is the valence band maximum) as a function of doping, together with photoemission energy distribution spectra (EDC's) and yield spectra for photon energies $\lesssim$ 6.2 eV. For Si (111)-2x1 they found a strong Fermi level pinning at the surface (E_F-E_V = 0.3 eV) due to surface states for a wide range of doping. They also saw different EDC's for the 2x1 and 7x7 surface structures, but could not unambiguously determine the surface state band positions due to the limited photon energy range. Direct spectroscopic measurements of the intrinsic surface state levels near E_V for Si (111)-2x1 were first reported by Eastman and Grobman[43] and by Wagner Spicer[44] using angle-integrated UPS. The experiments of Eastman and Grobman[43] on 5 Ω-cm (~10^{15} cm^{-3}) n-type Si revealed a single surface state band (which they attributed to the occupied DB surface

state) centered at about 0.5 eV below E_V, with a tail of states extending up to E_F (at 0.3 eV above E_V). Their EDC data for $\hbar\omega$ = 10 eV are depicted in Fig. 11.3a. The curve for clean Si (111)-2x1 shows the surface state peak, which disappears upon contamination. The difference curve between the two spectra represents the optical density of intrinsic surface states. The energy position of this peak was found to be constant in the photon energy range 10 eV to 20 eV, which is characteristic of emission from a narrow level as opposed to $\hbar\omega$-dependent features seen for Si bulk emission. The experiments of Wagner and Spicer[44] on 0.001 Ω-cm (10^{20} cm^{-3}) n-type Si revealed a strong peak at ∿0.6 eV below E_F togehter with a shoulder near E_V. These structures were identified as surface features by their sensitivity to oxygen exposure.

The discrepancies observed between the experiments of Eastman and Grobman[43] and of Wagner and Spicer[44] have prompted several further UPS studies on well characterized Si (111) surfaces.[23,45-49] The effects of cleavage steps have also been investigated.[49] It now seems clear that the clean cleaved Si (111)-2x1 surface shows a single surface state peak near ∿0.5 eV to 0.6 eV in angle-integrated PES measurements. The extra shoulder near E_V seen by Wagner and Spicer[44] appears likely to be due to either a volume emission contribution which could occur because of the extremely sharp band bending (∿12 Å) at the surface (of 10^{20} cm^{-3} n-type Si), or to extrinsic cleavage step effects.

The power of angular resolved photoemission was demonstrated by Rowe et al.[50,51] in a detailed study of the Si (111)-2x1 "dangling bond" surface state band. With the azimuthal emission angle fixed parallel to the $<11\bar{2}>$ direction of the crystal EDC's at various polar angles θ showed dramatic variations in the uppermost SS peak intensity, changes in energy and a splitting which occured

for θ greater than about 35°. A spectrum for θ = 25° (corresponding to the strongest SS peak intensity) is shown in Fig. 11.4b for clean and contaminated (111) surfaces, again demonstrating the preferential attenuation of the surface state feature. An important point illustrated in Fig. 11.4b is that angular-resolved photoemission can show greatly enhanced surface state emission (compared to angle-integrated photoemission) when the photon energy, electron energy, and electron momentum $\underset{\sim}{k}_{//}$ are suitably selected. In essence, one is preferentially reducing the bulk emission relative to the surface state emission, since few bulk state transitions occur near a given $\underset{\sim}{k}$ corresponding to a specific surface state.

Rowe et al.[50,51] also studied angle-resolved UPS from Si (111)-2x1 as a function of azimuthal angle, and found a marked three-fold symmetry pattern inconsistent with simple direct emission from a pure p_z dangling bond orbital. They also measured the surface state dispersion E vs $\underset{\sim}{k}_{//}$ in a $<11\bar{2}>$ direction[42,43] and found a band splitting, which is inconsistent with a simple dangling bond state. Several theoretical calculations, e.g. Pandey and Phillip[28,29,37] and Ciraci and Batra[45], have been used in attempts to understand the experimentally determined surface state bands. However, more theoretical and experimental work appears to be needed in order to unambiguously understand these surface bands (see also chapter 12 by Smith and Larsson in this book). At present, it appears that the observed surface state feature near the top of the valence band involve dangling bond orbitals and also back-bond orbitals.

In addition to Si (111)-2x1, Rowe and Ibach[52] have studied Si (111)-7x7, and Si (100)-2x1 surfaces using wide angle (cylindrical mirror analyser (CMA)) photoemission at $\hbar\omega$ = 21.2 eV. Besides the surface state feature near E_V, they observed a number of lower energy features which they associated

with surface states and surface resonances. Energy distributions for these three surfaces are depicted in Fig. 11.5. The data were taken at a photon energy of 21.2 eV. At these energies the effective electron escape depth is quite short for Si which implies a high surface sensitivity. Rowe and Ibach[52] took an average of the three spectra shown in Fig. 11.5, which they assumed, represented the bulk emission and then formed a difference spectrum between the experimental spectra of the various surfaces and this "bulk" spectrum. The difference spectrum was called an approximate surface density of state (see e.g. Fig. 3 in Ref. 52 for the 7x7 surface). In this way several surface features both near the valence band maximum and at lower valence band energies were identified.

This procedure is somewhat questionable on several grounds : (1) The CMA used did not accept a full 2π solid angle and anisotropic bulk $\underset{\sim}{k}$ -space effects are known to influence the observed spectra for different surfaces[53]. (2) The "exact" shapes (e.g., relative amplitudes of various features) are difficult to obtain and to reproduce for Si for $\hbar\omega \geq 20$ eV, and such amplitude variations will strongly affect the above-mentioned surface density of states. Nonethless, certain features in Fig. 11.5 seem to unambiguously be associated with intrinsic surface states. Namely, the -0.3 eV and -1.5 eV structures for Si (111)-7x7, the 0.5 eV structure for Si (111)-2x1, and the structure near 0 eV for Si (100)-2x1. However, other identified surface features (e.g. at -3.6 eV, -7.5 eV and -12.3 eV in Fig. 3 of Ref. 52) seem questionable at present and should be studied further with angle-resolved UPS. The existence of lower lying surface state features has been clearly established in energy loss spectroscopy (ELS) studies by Rowe and Ibach.[54] The interpretation of the occupied surface states rests heavily on the assumption that a single final state exists for all the surface state transitions on one surface. But no definitive description has yet been given.

For Si (111)-7x7 angle-integrated photoemission data by several groups[23,45-49] in addition to Ref. 52 (Fig. 11.5) show two occupied surface state structures near E_V in contrast to a single structure obtained for Si (111)-2x1. (See also Fig. 15 in Ref. 55.) A dominant feature is located about 1 eV below E_F and a second metallic-edge-like structure at E_F. Chiarotti et al.[7,56] have reported interesting infrared optical measurements for the Si (111)-2x1 and Si (111)-7x7 surfaces. For the former they observed strong infrared absorption with an edge at $\hbar\omega = 0.25$ eV and a peak at $\hbar\omega \cong 0.5$ eV, which corresponds to excitations from the uppermost occupied surface state DB band to the empty DB band. We discussed in section 11.2.1 that the DB band is split off in energy due to the reconstruction. For Si (111)-7x7, however, they find only a weak Drude-like absorption with no threshold.[56] Thus the optical data and photoemission data indicate that the Si (111)-7x7 surface can thus be thought of as a two dimensional metal whereas the (2x1) surface behaves more like a two dimensional semiconductor.

The origin of the transition from one of the various observed reconstructed surfaces into another appears to be not understood. Tosatti and Anderson[31] suggested that longitudinal surface phonons can couple strongly with electrons at the surface thereby distorting the surface lattice. Pandey and Phillips[28] have also looked for the possibility of some kind of Jahn-Teller distortion. More work is needed for an understanding.

Thus far we have discussed experimental results for the Si (111) cleavage face. There is much less information available for other Si surfaces. A recent theoretical discussion of models for the unreconstructed and reconstructed Si (100)-2x1 surfaces has been given by Appelbaum and coworkers.[57] This work contains references to earlier theoretical studies and to experimental results as well. An ideal Si (100) surface would have two broken bonds

per surface atom, and in reality the surface is reconstructed with a 2x1 superlattice. The calculations of Appelbaum et al.[59] favor a pairing model[58] over a vacancy model[59] for Si (100)-2x1. However, the geometry is not yet established for this surface, and LEED calculations indicate that both the above model geometries are probably incorrect.[60]

Noncleavage faces have to be prepared in a more elaborate way; either by molecular beam epitaxy or by repatative argon ion sputter etching and annealing to restore crystalline lattice order. The (100)-2x1 reconstructed surface has been studied by Rowe and Ibach[45,52,61] and by Sakurai and Hagstrum.[62] The UPS spectrum ($\hbar\omega$ = 21.2 eV) of Rowe and Ibach[45,52] shows a dangling bond surface state band 0.8 eV below the valence band maximum. The above-mentioned calculations[57] show also structure in that energy range, but which are also seem to be dependent on the choice of the surface geometry which is not accurately known.

We are not aware of any yield spectroscopy studies of intrinsic Si surface states by means of Si 2p core level-to-empty surface state transitions, although it is very tempting to do in view of the successful studies on III-V compounds as described in Section II.3. On a cleaved Si (111)-2x1 surface one would expect only a weak contribution to the yield due to transitions into empty dangling bond-type surface states, because of selection rules governing the optical transitions between the p-like core states and the empty states made up of p-like states and an admixture of s-like states (see section II.2.1). Electron energy loss (ELS) experiments, which yield similar information then yield spectroscopy, have been used to determine transition energies between the very narrow 2p core states and final empty surface states. Koma and Ludecke[63] determined the location of the empty surface states for the Si (100)-2x1 surface just above the Fermi level which is taken

to be about 0.3 eV above E_V. Surface features have also been found on the Si (111)-7x7 surface and as usual, the surface features were identified by their sensitivity to oxygen adsorption. Due to the very small penetration depth of the primary low energy electrons the ELS technique is exceedingly surface sensitive. However, as with yield spectroscopy (see section II.2) or any other "optical transition spectroscopy" involving core states, the effect of excitonic binding energy shifts have to be considered very carefully, when absolute one-electron energies are to be derived from the spectra. Very recently core exciton effects in the order of ∿1-2 eV on Si (111)-7x7 surfaces have been reported.[64] For the corresponding bulk transitions (2p- to empty conduction band states) excitonic binding energies in the order of 0.9 eV have been estimated.[64] To our knowledge no calculation of such excitonic binding energies have been made.

In summarizing results for Si surfaces, many surface state features - both occupied and empty - have been established and investigated experimentally and theoretically. However, more work is needed for a detailed understanding even for the surface states near the band gap, but especially for the lower-lying surface states. A general inability to accurately and unambiguously determine semiconductor surface atom positions is an outstanding problem at present.

II.2.3 Intrisic Surface States on Germanium

Germanium has been studied much less extensively than silicon. Nevertheless, a degree of understanding of Ge surface properties has been achieved. This has been facilitated by the general similarity of the bulk crystal and electronic properties of Si and Ge.

In the first surface band structure calculation for the ideal Ge (111) surface (see Fig. 11.1), Hirabayashi[65] used a tight binding approach and determined a surface state band about one eV wide with its center very close to the valence band maximum E_V. Pandey and Phillips[37] and Chadi and Cohen[66] also studied Ge (111)-1x1 using a tight binding method, but with more realistic parameters than used previously.[65] The latter calculation[66] showed already for the ideal Ge (111) surface deep lying surface states (more than 5 eV below E_V) as well as resonant states in addition to the dangling bond surface state band. This is similar to the behavior for the ideal Si (111) surface.[41]

Upon relaxation, additional surface states associated to the backbonds to the second surface layer atoms appear and a considerable change in energy position (∿1 eV) of the dangling bond band occurs. No surface band structure calculations for the Ge (111)-2x1 reconstructed surface appears to be available.

The LEED analysis of Lander, Gobeli and Morrison[22] showed that the 2x1 superstructure found for a cleaved Ge (111) surface converts to a 2x8 superstructure by annealing (above 300° C). Gobeli and Allen[4] first postulated empty and occupied surface states for Ge (111), based on their photoyield and contact potential measurements. Eastman and Grobman[43] were the first to give direct experimental evidence on occupied surface states on the (2x1) surface by means of photoelectron energy distributions. Their angle-integrated UPS results for $\hbar\omega$ = 10.2 eV are depicted in Fig. 11.6a which show a band of surface states about 1 eV wide centered at about 0.7 eV below the Fermi level. In Fig. 11.6a the Fermi level at the surface of the 4×10^{14} cm^{-3} n-type Ge sample, with $(E_C-E_F)_s$ = 0.25 eV in the bulk, lies very close to the top of the valence band; this implies an upward surface state band banding of ∿0.4 eV and a strong Fermi level pinning. Murotani and coworkers[67] have studied cleaved and annealed Ge (111) surfaces by means of UPS energy distribution

measurements at $\hbar\omega$ = 10.2 eV. They observe a single surface state band for the Ge (110)2x1 surface which agrees in width and position with the results of Eastman and Grobman.[43] Also, they observed that the DB structure changed to a double peaked structure for a partially annealed surface, and then with additional annealing turned back again into a single peak for the Ge (111)2x8 superstructure. This is in contrast to the Si (111)7x7 surface, where two surface state peaks are observed at the upper valence band region (subsection 11.3.2).

Using ultraviolet photoemission spectroscopy at $\hbar\omega$ = 21.2 eV Rowe[68] has reported five intrinsic surface state structures on Ge (111)2x1 which he interpreted as due to dangling bonds (i.e., the state described above) or to back bonds between first and second atom layers. As in the previously described experiments on Si the surface nature of the observed structures was investigated with its sensitivity to chemisorption of atomic hydrogen. Interestingly, the same surface state peak positions were detected with different intensities on both low step density 2x1 surfaces and on high step density surfaces, which did not show 2x1 reconstruction, but only a splitting of the integral order LEED spots. Concerning the lower-lying backbond surfaces states reported by Rowe[68], it appears certain from the data presented that several structures (e.g., peaks A_3 and A_3') are surface associated features. However, other features (B_1 and B_2) are degenerate with bulk Ge structures as well as Ge+H structures and thus there appears to be insufficient data presented to unequivocably establish those structures as intrinsic surface states. The interesting observations of Rowe[68] for Ge (111) warrant further studies.

Very recently Chiarotti and Nanarone[69] applied an electric field modulated internal reflection technique to the study of the Ge (111)2x1 surface. As

in their earlier experiment[7] they observed infrared optical transitions between an occupied surface state band and an empty surface state band, where these dangling bond states are in analogy to Si split by the (2x1) reconstruction (as discussed for Si (111)2x1 in section II.3.2). In their analysis Chiarotti and Nanarone[69] favored the buckled surface model of Haneman[26] with raised atoms negatively and lowered atoms positively charged.

Evidence for empty surface states on the cleaved Ge (111) surface has been obtained by Eastman and Freeouf[18] using the technique of partial yield spectroscopy and by Rowe[9] using ELS. Optical transitions are generated from the Ge 3d core states into empty surface and conduction band states. Due to spin orbit splitting of the core state, two surface state peaks are seen (Fig. II.6b) just below the onset of the bulk 3d transitions. They disappear upon a monolayer coverage of Sb. Within a one-electron approximation the center of the empty surface state band lies about 0.1 eV above the valence band maximum. But most likely an excitonic binding energy shift is involved in the optical transitions which implies that the "true" position of the dangling bond surface state peak observed in this way is located at a few 1/10 eV at higher energies. We shall discuss this problem in more detail in Section II.3.3.

CEL experiments[8,9,70,71] with electron energies of less than 200 eV have also been used to study surface state transitions on various Ge surface. Empty as well as occupied surface states have been detected. Ludecke and Koma[70,71] derived that Ge empty dangling bonds exhibit p-like character on the (111)8x8 surface and mixed s-p character on the (100)-2x1 surface; however, Freeouf[72] pointed out that there is considerable ambiguity in these findings[70].

In summary several occupied surface states have been observed on the cleaved Ge (111) surface with a wide range of valence band energies. As with Si,

additional work (e.g., angular-resolved photoemission measurements and calculations for reconstructed surfaces) is needed to better understand the surface electronic properties of the various Ge surfaces.

II.3 Intrinsic Surface States on Compound Semiconductors

To date, GaAs has been the most extensively studied and technologically important compound semiconductor. Most experimental and theoretical surface studies have considered the homopolar (110) surface of the zinc-blende semiconductors. In this section we mainly describe photoemission surface studies of the intrinsic GaAs(110) surface, together with relevant surface band calculations. Nonpolar III-V semiconductor surfaces and II-VI surfaces are briefly described.

II.3.1 Surface Geometry and Electronic Structure

The natural cleavage face of the zinc-blende semiconductors is the (110) face. The surface geometry and the surface BZ of homopolar GaAs(110) are depicted in Fig. II.7. Geometrical configurations for both the "ideal" surface as well as for a "fully relaxed" surface are shown[73,74]. The latter is characterized by the surface As anions moving out and the Ga cations moving in (with a 35° bond angle (η) change and with constant bond lengths assumed) so as to form a planar arrangement. This relaxation, which is similar to the "buckling" of the Haneman model[26] described for Si(111)-2x1, results in a surface sp^2 hybridization, compared with sp^3 hybridization for the ideal surface. Using low energy electron diffraction (LEED) MacRae and Gobeli[73] first showed that the GaAs(110) surface is relaxed. Recently Lubinsky et al.[74] confirmed these findings with their dynamical LEED intensity analysis. They have definitely shown that GaAs(110) surfaces have a significant relaxation while retaining the bulk (1x1) periodicity. The same authors[74] have further concluded that the fully relaxed geometry described in Fig. II.3 occurs. However, the accuracy of these difficult calculations is insufficient[37] to rule out other relaxed geometries such as somewhat smaller bond angle changes, bond length changes etc.

Theoretical calculations of the local density of states (LDOS) for ideal and relaxed GaAs(110) surfaces are shown in Figs. II.8 and II.9. The general concepts of the LDOS and their importance as well as descriptions of the self-consistent pseudopotential calculations by Cohen and coworkers[75] (Fig. II.8) and the tight-binding calculations by Pandey[76] (Fig. II.9) are given by Forstmann in chapter 8 of this book and in Refs.34,35. In Fig. II.8a) the local density of states of layer 5 already represents that of the bulk solid for the 12 layer slab model calculation[75], while the LDOS of the outer-most surface layer 1 is seen to differ significantly from the bulk. In Fig. II.8b) and II.8c) the LDOS's for layer 1 are given for the ideal and fully relaxed surface geometries as described in Fig. II.7. In Fig. II.9a) the LDOS of layer 10 represents that of the bulk for the tight binding model calculation[76], while Fig. II.9b) and II.9c) and II.9d) give the LDOS of the surface layer for the ideal surface, a "partially relaxed" surface (bond angle change $\eta = 19^{\circ}$) and a "fully relaxed" surface ($\eta = 35^{\circ}$ in Fig. II.7). An earlier tight-binding calculation by Joannopoulus and Cohen[77] gave results for the ideal surface qualitatively similar to those in Figs. II.8 and II.9. For both calculations, the LDOS of layer 1 for the ideal surface is seen to differ significantly from the bulk DOS, with a sharp occupied state B_1 lying near the valence band maximum E_V and a sharp empty band B_1' lying ~ 1 eV above E_V, i.e. in the 1.4 eV band gap. Detailed analysis shows that B_1 is mainly an As derived p-like dangling bond state, while B_1' is mainly a Ga derived dangling bond state.

Previously, states B_1 and B_1' have been qualitatively described within the bond orbital model of Harrison and coworkers[78] (GSCH model)[79,80] for ideal (110) surfaces. Within this model, the termination of the bulk lattice causes the anions of the surface atoms to carry approximately two electrons, which do not participate in the bonding within the sp^3 hybrid (see Fig. 11.7). They form the occupied dangling bond states. The cations contribute their electrons to the bonding to the three nearest neighbors. The cations therefore give rise to the empty DB states. The DB surface states for the zinc-blende lattice have also been studien in several other theoretical investigations of the surface band structure[81,82].

Referring to Fig. 11.9, in addition to states B_1 and B_1' three lower energy surface state bands B_2 (mainly bonding As p-like), B_3 (mainly As p-like plus Ga s-like) and B_4 (mainly As s-like) occur depending on the surface geometry. As seen in Fig. 11.8 and 11.9 relaxation of the surface layer has a striking effect on the LDOS of the surface. In particular, the As-derived state B_1 moves down into the valence band, while the Ga-derived empty state B_1' moves up towards and into the conduction bands. Bands B_3 and B_4 occur for all geometries[75-77], with B_3 being a free surface state only in limited regions of the surface BZ. Band B_2 exists as a free surface state in a limited region of the BZ near $\bar{X}'$ for the relaxed surfaces[76]. Many of these features are seen in experimental photoemission studies of these occupied and empty surface states, which shall now be described.

11.3.2 Occupied Surface States on GaAs(110)

We begin our discussion on surface states on compound III-V semiconductors with the angle-resolved experiments on GaAs(110) by Knapp and Lapeyre [83]. Angle resolved PE studies of GaAs(110) with synchrotron radiation (see chapter 15 of this book) by Lapeyre and Knapp[83] have permitted both the identification of two occupied surface states, B_1 and B_3*), as well as the energy dispersion ($E(\underset{\sim}{k}_{//})$) of the surface state band B_1 for a portion of the surface BZ. These surface states had not been previously determined in angle integrated photoemission measurements, mainly due to their degeneracy with the bulk valence band emission.

As described in Section 11.1 the surface state dispersion $E(\underset{\sim}{k}_{//})$ can be directly determined from the measured surface state energy and the wave vector $\underset{\sim}{k}$ of the photoelectron as determined by the electron analyzer. A set of such measurements for GaAs(110)[83] showing emission from the surface state band B_1 and its $\underset{\sim}{k}_{//}$-dispersion in the $\bar{\Gamma}$-$\bar{X}$ direction (see BZ in Fig. 11.7) are given in Fig. 11.10. The uppermost peak, identified as B_1, was shown to correspond to a surface state by its sensitivity to surface contamination. In Fig. 11.10 $\underset{\sim}{k}_{//}$ increases with increasing photon energy $\hbar\omega$ (i.e. increasing kinetic energy E_k) since the emission angle (Θ,Φ) was held fixed. The dispersion E vs $\underset{\sim}{k}_{//}$ in the $\bar{\Gamma}$-$\bar{X}$ direction (see state B_1 was determined from the data such as that in Fig. 11.10, and is shown in Fig. 11.11 for a range of $\underset{\sim}{k}_{//}$-values spanning two surface Brillouin zones (repeated zone scheme).

For comparison we show in Fig. 11.11 also calculated E vs $\underset{\sim}{k}_{//}$ curves for the B_1 state by Joannopoulus and Cohen[77] for the ideal surface and by Pandey for the 19° relaxed surface [76] (see Fig. 11.9). General agree-

*) We use a different notation of the surface states than in Ref. 77 and Ref. 83.

ment is seen between the experimentally determined dispersion curve and the the one calculated for the relaxed surface with a somewhat larger dispersion seen in the experimental curve. This is believed to be due to the the fact that the experimentally determined curve contains structure due not only to the state B_1 but also due to the state B_2. As previously mentioned, the second surface state B_2 exists near $\bar{X}'$ and lies slightly lower in energy than state B_1 by about - 1.0 eV. Thus the measured spectrum likely includes contributions from both states for $\underset{\sim}{k}$ near $\bar{X}'$, which is just where ($\hbar\omega$ - 18 eV) the two peak structure is seen in Fig. 11.10.

The third surface state band B_3 is a true surface state near $\bar{M}$ in the BZ and has also been detected in angle-resolved measurements such as shown in Fig. 11.12[83]. The level labeled B_3 was determined to be a surface state by its sensitivity to absorbed hydrogen. A 0.1 Torr sec exposure of H_2 results in an obliteration of the B_3 peak (see Fig. 11.12). Even with angular-resolved photoemission experiments it has not been possible, up to now, to identify the lowest lying surface state band B_4, which is As s-like.

Surface state emission of occupied states can also be observed in angle integrated photoemission spectra, although in general with much more ambiguity than in angle resolved spectra. This is illustrated in Fig. 11.13, where "angle integrated" photoemission energy distributions for $\hbar\omega$ = 30 eV and 1486 eV [84] are shown*). For $\hbar\omega$ = 30 eV, the effective escape depth $\ell(E)$ of photoelectrons in GaAs is near its minimum value (4-6 Å)[85], while at $\hbar\omega$ = 1486 eV $\ell(E)$ is about 3 to 5 times as long. Thus, neglecting matrix elements, the latter can be considered to approximately reflect features in the bulk valence band density of states, while the former can be expected to also reflect surface state features.

*) To facilitate the comparison we have subtracted a background of secondary electron emission for both curves. The 30 eV spectrum was taken with a cylindrical mirrow analyser, while the XPS spectrum[84] was measured with a sperical analyser.

By comparing the two curves in Fig. 11.13, differences that can be associated with surface state features are seen in the $\hbar\omega$ = 30 eV spectrum. Namely, the sharp peak at -1.1 eV ist attributed to the maximum in the LDOS of the surface band B_1, the shoulder near -2 eV might be due in part to the surface band B_2, and the bottom of the valence band (As s-band with very weak emission) is shifted upwards by ~ 1 eV. The latter feature, which is experimentally uncertain due to its weak emission and observed surface sensitivity is consistent with the results of theoretical calculations reproduced in Figs. 11.8 and 11.9. A weak shoulder structure in the 30 eV curve near -5.5 eV coindicdes with the energy of the surface state level B_3, but this structure is sufficiently weak in the angle-integrated spectrum to preclude a definite association with B_3. Similar spectra than that shown in Fig. 11.13 for GaAs(110) have been observed for other III-V semiconductor (110) surfaces[85,86] indicating the general occurrence of occupied surface states in the upper valence band region.

In summary, both angle resolved and angle integrated photoemission measurements show several occupied surface state bands, with the uppermost As-p dangling bond state lying between ~ 0.5 eV and 1.2 eV below the valence band edge. By comparison with calculated LDOS's, this energy position is seen to be consistent with a significantly relaxed surface geometry and inconsistent with an ideal surface geometry.

11.3.3 Empty Surface States on GaAs(110)

We now disucss several applications of yield spectroscopy to the study of empty surface states on GaAs(110). For all types of yield spectroscopy, the photon energy is scanned rather than the electron energy (in CIS, $\hbar\omega$ and E_k is scanned). In Section 11.1 we have already described

the physical processes involved in the various techniques as well as the experimental methods to implement them. In this section some specific examples are discussed.

Three complemental types of yield spectroscopy are shown in Fig. 11.14:

(a) a partial yield spectrum (PYS or equivalently constant final state spectrum (CFS)),

(b) a constant initial state (CIS) spectrum and

(c) a total yield spectrum Y(hω) together with a derivative spectrum $\partial y/\partial\hbar\omega$ (Fig. 11.14d).

All spectra show a pair of sharp peaks at $\hbar\omega$ = 19.5 eV and 20 eV which corresponds to the spin orbit split Ga(3d) to empty surface state transitions [18,86-88]. As previously explained all the above yield spectra show the core level to surface state excitation spectrum if the optical excitation and the core level deexcitation and exciton recombination processes are uncoupled. The ratio of the surface to the background contribution, however, can be varied by the choice of the experimental parameters. In the PYS in Fig. 11.14a), [87] a kinetic energy of 4 eV was used in order to avoid spectral contribution due to primary valence electrons but still be surface sensitive. In the CIS depicted in Fig. 11.14b) [86], the empty surface state transitions are enhanced by setting the initial energy to the minimum of the valence band emission. This energy (E_i = 6 eV) corresponds also to a strong contribution of Auger electrons for photon energies close to the Ga(3d) surface state transitions. In the total yield spectrum in Fig. 11.14d), the Ga(3d) to surface state transitions are observed with about the same surface state-to-background emission ratio as seen for the PYS in Fig. 11.14a). We note that from the experimental point of view, the total yield technique is much simpler than the others in that an electron energy analyser is not required. We also show a total yield derivative spectrum in Fig. 11.14d), which enhances the two surface state transition peaks. The spin orbit splitting of the 3d core states of 0.45 eV and the line width of the d5/2 component of 0.25 eV can easily be determined from this spectrum. Weaker but relatively sharp transitions occur at higher energies.

Direct evidence that the two sharp yield spectrocopy peaks at ~ 19.5 eV and 20 eV correspond to surface state peaks is given in Fig. 11.14c) [18], where we compare the partial yield spectrum from Fig. 11.14a) with the bulk absorption edge spectrum due to Gudat et al. [89]. In both spectra, a background due to valence electron excitations is subtracted out. The sharp surface state peaks are seen to be missing in the absorption spectrum. Also various adsorbates (oxygen) and metallic overlayers (Au, Sb etc.) cause the intrinsic surface state peaks to disappear or become highly modified [86,90], thus indicating that they are associated with empty surface states. As discussed above, an additional characteristic of the lowest empty surface state level on the III-V semiconductors is that they are mainly cation derived, i.e. Ga-derived for GaAs(110). This can be determined experimentally by measuring yield spectra for photon energies corresponding to both Ga(3d) → surface state excitation and As(3d) → surface state excitations. The latter spectrum will show no structures due to transitions into empty surface states. This behavior has been reported for GaAs(110) using partial yield spectra [87,88] and for GaAs(110) using electron energy loss experiments [8], which can be interpreted in about the same way as yield or absorption spectra.

In a one-electron picture, the empty Ga-derived surface state level would be located in the fundamental band gap at about 0.9 eV above the valence band maximum and would be quite narrow ($\lesssim$ 0.25 eV). This energy position is determined by taking $\hbar\omega_s - E_B(d5/2)$ = (19.5-18.6) eV,

where $\hbar\omega_s$ is the photon energy corresponding to the surface state transition peak and $E_B(d5/2) = 18.6$ eV is the Ga(d5/2) core level binding energy referred to the top of valence band. However, it has been shown by Huijser and van Laar[91] and by Gudat and Eastman[86,92] from band bending measurements for n-type ($2\cdot10^{17}$ cm^{-3}) GaAs(110) that there is not a high density of empty surface states in the band gap, i.e. $\leq 10^{-3}$ states/atom. This implies that the empty surface state level must lie above the conduction band minimum E_c and that a large excitonic binding energy ($\delta E_{EX} \geq 0{,}6$ eV) occurs for Ga(3d)-surface state transitions. In view of the negligible width of the d-core states ($<$ .01 eV)[93] and the sharp line-shape observed for the surface state transition peak, the surface state might be quite narrow. However, the strong excitonic effects which occur make such a conclusion uncertain. In agreement with our findings, very recently Guichard and coworkers[20] found the position of the valence band edge with respect to the Fermi level to be the same at the surface and in the bulk of intrinsic n-type GaAs(110), i.e. a flat band condition with E_F - 0.07 eV below the conduction band for $2\cdot10^{16}$ cm^{-3} doping. They concluded from their yield spectroscopy experiments ($\hbar\omega < 7$ eV) that there is a band of occupied surface states in the gap with a very small density of states, and that ~ 1 Langmuir of oxygen exposure (which should correspond to ~ 10^{-7} monolayers) obliterates those states. In other studies[79,80,87,91] a behavior consistent with these results has not been observed.

Excitonic effects are also seen in the intensity ratio of the d(5/2) to d(3/2) spin orbit components. The observed ratio is about 0.7 rather than 1.5 as expected from the d(5/2)/d(3/2) degeneracy ratio using the j-j coupling scheme. Using the formalism developed by Toyozawa and Onodera Freeouf[72] has analysed these line intensities and has concluded that there is a small but significant exchange interaction between the excited electron and the remaining d-core hole.

Lapeyre and Anderson[94] have studied excitonic effects for GaAs(110) using CIS spectroscopy. They first showed the existence of dramatic polarization-dependent excitonic effects. In Fig. II.15 constant-initial state spectra are shown for s- and p-polarized radiation . Spin-orbit split Ga(3d) → surface state transitions are again seen at $\hbar\omega$ = 19.5 eV and 20 eV. However, for the initial energy (E_i = -1.2 eV) which was used, striking differences in lineshapes and intensities occur. These are due to electron emission resulting from direct recombination, which can be separated from direct Auger emission by using a small initial energy ($E_i < 2E_{gap}$) so that there is no Auger electron contribution . In the direct recombination process, the core hole-surface state electron pair directly recombines and gives the recombination energy ($\sim \hbar\omega_s$) directly to a valence band-conduction band electron hole pair via a coulomb interaction. This process is only expected to be strong if there is a strong interaction between the core hole and excited electron (i.e. an excitonic effect). The complicated polarization and lineshape characteristics depicted in Fig. II.15 are not fully understood at present. Part of the structure has been described by Pandey and Phillips[95] on the basis of their nonlocal structure calculation.

We now briefly summarize intrinsic surface state features for GaAs(110). First, there is a relatively narrow occupied surface state band in the range ~ 0.5 to 1.5 eV below E_V which corresponds to an As p-like dangling bond state. This state was first seen in angle-resolved measurements (Fig. II.10) and has also been seen in angle-integrated measurements (Fig. II.11). Second, there is an empty surface state level just above

the conduction band minimum which exhibits a very narrov lineshape for Ga(3d) core level to surface state transitions as well as a large ($\gtrsim$ 0.6 eV) excitonic binding energy. Lower lying occupied surface state features have also been observed, notably the surface state level B_3 for surface momentum $k_{\parallel}$, near the corner ($\bar{M}$) of the surface BZ, as well as a narrowing and shifting to higher energies of the lowest As s-like valence band level for the surface layers relative to the bulk. All of these surface state features can be semi-quantitatively described by the surface state calculations (e.g. Fig. 11.8 and 11.9), but only if a significant surface relaxation is assumed. It is clear from this comparison together with the LEED analysis that such a relaxation occurs with bond angles changing so that the As atoms move outwards and the Ga atoms move inwards. The exact relaxation, including possible bond length changes, is not yet conclusively established, but is believed to be at least as much as $\eta = 19^{\circ}$ (see Fig. 11.7, which shows the geometry for a maximum rotation of η=35°), for which tight binding calculations give occupied As p-like and sharp Ga s- and p-like surface states in good agreement with experiment (Fig. 11.9).

11.3.4 Trends and Correlations on Surface States of III-V Semiconductors

Using yield spectroscopy empty surface states have been studied for a number of cleaved (110) surfaces of III-V semiconductors[86-88] These measurements are summarized in Fig. 11.16 for six semiconductors and show interesting trends. In Fig. 11.16, E_S denotes the measured one-electron energy of the surface state peak (without excitonic corrections, i.e., $E_S = \hbar\omega_S - E_B\ (d_{5/2})$ and is measured relative to E_V) and the dashed lines schematically represent the bulk density of states with E_V and E_C denoting the valence and conduction band edges and X_1 and L_1 being the low lying bulk conduction band critical-point band energies. A solid triangular-

like curve roughly denotes the measured width of the surface state transitions as determined from partial yield experiments (including core level broadening), E_F denotes the Fermi level at the surface (of lighty doped n-type samples), and E_o denotes the Fermi level position at the surface with a metal overlayer present. Thus $(E_c - E_o)$ corresponds to the Schottky barrier interface energy.[96] One observes in Fig. 11.16 that there is no simple correlation in the surface state energy E_S and the fundamental gap $E_C - E_V$. There are, however, correlations between E_S and both conduction band energies and valence band energies. These correlations between the various quantities discussed above can readily be seen from table 11.3. Notably, E_S lies $\sim$1.1 eV below the X_1 critical point and is about 0.4 eV above E_o for all six semiconductors. McCaldin et al.[97] have shown that also $(E_S - E_V)$ and $(E_o - E_V)$ vary systematically with the anion electronegativity.

Considering the large excitonic binding energy $\delta E_{ex} \gtrsim 0.6$ eV, which has been established for GaAs(110), the empty surface states for GaSb, GaAs, InSb, InAs and InP all lie above E_V, i.e. not in the band gap. The Fermi level positions for GaP and InP in Fig. 11.16 are those determined in the recent work by van Laar et al.[98]. They find for GaP(110) - in contrast with the 5 above mentioned III-V semiconductors - that there is a strong Fermi level pinning at $\simeq$ 0.5 eV below E_c. This pinning is attributed to intrinsic surface state pinning, and implies that for Ga(3d) → surface state transitions for GaP (110) there is an exciton binding energy in the order of 0.6 eV, i.e. the same as concluded for GaAs(110).[86]

Thus far we have discussed surface electronic properties of cleavage faces of III-V compounds. We now turn to a brief discussion on non-cleavage faces of III-V compounds and we will finish this section with a comment on II-VI compounds.

Non-cleavage faces have to be prepared by molecular beam epitaxy (MBE) or by argon ion sputter etching and annealing, Polar faces can be stabilized with different surface superstructure depending on the experimental conditions. For example, the polar GaAs ($\bar{1}\bar{1}\bar{1}$) As surface can be prepared in three stable and ordered states (two by MBE and one by ion bombardment), whereas the GaAs (111) Ga surface is only obtained in a 2x2 superstructure.[99] The three ($\bar{1}\bar{1}\bar{1}$) As surfaces differ in their As concentration of the first atomic layer. Ranke and Jacobi[99] found surface sensitive structures at ∿1.6 eV and ∿3.5 eV below the valence band maximum for the three ($\bar{1}\bar{1}\bar{1}$) As surfaces from angular-resolved photoemission at $\hbar\omega$ = 21.2 eV. The intensities of the structures varied strongly with the As-surface concentration. Ranke and Jacobi explained the structures as due to occupied surface states derived from As states. Ludeke and Esaki[8,71] found also filled surface states on GaAs ($\bar{1}\bar{1}\bar{1}$) As from ELS measurements which they interpreted as As dangling bond states. But they estimated the surface states to lie 0.1 to 0.4 eV above the valence band maximum, which indeed was in agreement with angle integrated photoemission results of Ranke and Jacobi[100], who found filled surface states in the lower half of the band gap, but in disagreement with the angular resolved UPS results described above.[99] Ludeke and Esaki also determined empty Ga derived dangling bond surface states to lie in the band gap of GaAs (111) Ga and GaAs (100). We note that these energy positions are derived from a single-particle description, i.e., excitonic effects, which are important for ELS[64], are neglected. Empty, cation derived and filled, anion derived, surface states have been measured for Ga- and

P-rich GaP ($\bar{1}\bar{1}\bar{1}$) P surfaces using ELS at 100 eV and photoemission ($\hbar\omega$ = 4.5 to 6.6 eV)[101]. The experimental findings on the polar faces of GaAs and GaP appear to confirm the results of theoretical calculation[56,152] and to support the bond orbital model (GSCH model, see Sec. 11.3) which was modified by Spicer et al.[79,80,103] to include all crystal faces of III-V compounds. Very little work is available for II-VI compounds. In theoretical studies trends with semiconductor ionicity have been studied[66,75,77,102,104] supporting the model of ionic surface states.[104] Core level to empty surface-states transitions have been observed for ZnS (110) and ZnSe (110) using partial yield spectroscopy.[105] In general, the situation on non-cleavage faces of III-V compounds and on II-VI compounds is less well established. A lot more work is needed for an understanding.

11.4 Chemisorption and Extrinsic Effects on Semiconductor Surfaces

An understanding of the intrinsic surface properties, which we have discussed in the previous sections for ideal, relaxed and reconstructed surfaces of group IV and compound semiconductors, is fundamental. Extrinsic effects[106] like impurities or imperfections at or near the surface, cleavage steps or various kinds of adsorbates are, however, of great practical importance. In experimental studies it is extremely difficult to avoid any contribution of extrinic effects to the spectra and often it is also difficult to separate extrinsic from intrinsic effects. As an example see e.g. the discussion on Si (111)2x1 photoemission experiments given in Sect. 11.2.2. An outstanding technological importance of metal induced extrinsic effects is present in the formation of Schottky barriers. In Sec. 11.3.4 we briefly touched this topic. A detailed study of Schottky barrier formation is beyond the scope of this article. The theoretical situation of this problem, which on the whole does not appear to be satisfactory, is briefly described in references 34 and 82. The experimental situation on Si (111)7x7 has been

recently discussed.[107] In this section we discuss two examples of the many chemisorption and extrinsic effects observed: 1. The effect of cleavage steps on the surface electronic properties of Si (111) and 2. chemisorption of hydrogen on Si (111) surfaces. These examples appear to be fairly well understood. The situation on the early stages of the oxidation of compound semiconductor surfaces seems somewhat unclear, although a lot of experimental results are available obtained with photoemission as well as with other techniques.[79,80,86,99,108-110] Further work is in preparation. Often the experimental results contradict each other and different structural models are used to explain the data. LEED intensity measurements, which have proven to be a powerful tool in structural analysis, can not be used for the study of oxygen on semiconductor surfaces, since adsorbed oxygen dissociates by electron irradiation.[111] Theoretical calculations appear not to be available.

The importance of surface defects on the distribution of electronic surface states has long been realized.[106] For GaAs (110) it has been suggested that surface steps on poor-quality cleavages may play an important role in determining the surface state distribution as seen with UPS.[18,78] Band bending measurements[86,91] on GaAs (110) definitely showed that changes in the surface potential (E_F-E_V) by almost 1 eV occured depending on the quality of the cleave. The first experimental correlation of surface steps observed by LEED techniques and surface state energy distribution measurements by UPS has been given by Rowe and coworkers[49] on cleaved p-type Si (111). Their photoemission results for two clean surfaces with a high step-atom density ($\sim$ 10 %) and a low step-atom density ($\sim$ 3 %) are shown in Fig. 11.17 for a photon energy of 21.2 eV. The low-step-density surface has a single broad maximum at 0.9 eV below E_F in agreement with the results described in Sect. 11.2.2 and displayed in Fig. 11.4a. The high-step-density surface, however,

has an additional shoulder-like structure at about 0.5 eV below E_F extending into the band-gap region. This is similar to the observations on Si (111)7x7 which is thought of as a two dimensional metal. For comparison a spectrum of the same Si (111) surfaces but covered with $\sim$1 monolayer of atomic hydrogen is also shown in Fig. 11.17 demonstrating the surface sensitivity of the observed structures. Curves a (low-step density) and c (H covered) in Fig. 11.17 have been shifted by +0.25 eV and +0.35 eV to align E_{VB} and thus to account for the apparent changes in band-bending (E_F-E_V). In addition to the dangling-bond surface states also back-band surface states were found to depend on the step density.[49]

Henzler[106,112,113] has determined the step height and terrace width on Si(111). He found that the step height is 3.01 Å, which is slightly less than the height of two amic layers (3.14 Å). Of the two possible steps on Si (111) surfaces - one with one dangling bond and the other with two dangling bonds - only edge atoms with two DB have been observed.[113]

Calculations of the electronic structure of a stepped Si (111) surface have been presented.[29,114,115] Rajan and Falicov[114] used a tight binding and Schlüter et al.[115] used the self-consistent pseudopotential approach with a model structure of Si (111) containing double layer steps. In both calculations it is found that the DB surface states are strongly affected by steps and that additional structure in the density of states is obtained in the vicinity of the fundamental gap. The step states appear both above and below the Si (111)2x1 intrinsic surface states and are correlated to the structures indicated in Fig. 11.17. The step-state structure at about -1.5 eV below E_F which is more clearly seen in the exaggerating difference curve shown in Fig. 5 of Ref. 103, is mainly associated with edge atoms with two

dangling bonds. The peak at the valence band edge is attributed to contributions of various step atoms with one dangling bond.[115] Both calculations find a 0.3 eV Fermi level lowering with respect to E_V on high-step density (111) surfaces in agreement with the experiment.

Chemisorbed hydrogen on Si (111) has been extensively studied both experimentally using UPS[25,61,116] and theoretically[25,117,118]. Two phases of chemisorbed hydrogen have been identified and analyzed: a monohydride phase Si (111):H obtained from a Si (111)7x7 surface[116], and a trihydride phase Si (111):SiH_3 obtained from quenched Si (111)1x1.[25] UPS spectra[25] measured at $\hbar\omega$ = 21.2 eV for clean Si (111)1x1, for Si:H, and Si:SiH_3 are displayed in Fig. 11.18. The main difference of the Si (111)1x1 spectrum to that of the 7x7 spectrum is that the valley at $E-E_{vac}\simeq-10$ eV is shallower. The two maxima (labeled C and D) of the Si:H spectrum appear in the early stages of the atomic hydrogen exposure. Upon continued H-exposure (90 min) peaks C and D completely disappear and new structures A and B appear. Calculated UPS spectra[25,118] for both Si-H chemisorption phases are also shown in Fig. 11.18 for comparison and are seen to be in a remarkable agreement with experiment, e.g., compare the hydrogen induced features A to D. These spectra were calculated using an LCAO tight binding method and a molecular model for chemisorbed hydrogen.[25] These theoretical studies have concluded that H and SiH_3, respectively, bond directly on top of the surface Si atoms for the Si (111):H and Si (111):SiH_3 phases. The Si:H system appears to be one of the best understood extrinsic semiconductor surface state systems; however, it would be interesting to perform LEED and infrared energy loss spectroscopy studies of Si:H vibrational modes in order to further confirm these structural models. Hydrogen chemisorption has also been studied experimentally on the Si (110)5x1[119] and on the Si (100)2x1[62] surfaces. Hydrogen on Ge (111) has been investigated experimentally using UPS[61] and theoretically.[118]

11.5 Conclusions

In this article we have described various photoemission techniques currently being used to the study of surface electronic properties of semiconductors. We have discussed selected results of recent experimental and theoretical studies; mainly on the Si, Ge and GaAs cleavage faces where, at the present time, most data exist on intrinsic surface states. Also intrinsic surface states of non-cleavage faces of group IV and III-V semiconductors have been included in the discussion. Just two examples - cleavage steps and hydrogen chemisorption - of the many extrinsic effects were presented. We have seen that even the most thoroughly studied intrinsic Si(111) surface is not understood in detail. This holds for the surface states near the band gap, but especially for the lower lying surface states. A general inability to accurately and unambigously determine semiconductor surface atom positions is an outstanding problem at present.

Acknowledgments

The authors gratefully acknowledge valuable conversations with K. C. Pandey and they are indebted to him for making his results available to us prior to publication. We thank Mrs. E. Thumann and Mrs. K. Schmöger for the careful typing of the manuscript.

References

1. J. Bardeen, Phys.Rev. 71, 717 (1947)
2. F.G. Allen and G.W. Gobeli, Phys.Rev. 127, 150 (1962)
3. F.G. Allen and G.W. Gobeli, J.Appl.Phys. 35, 597 (1964)
4. G.W. Gobeli and F.G. Allen, Surface Sci. 2, 402 (1964)
5. see e.g., P. Mark, Surface Sci. 25, 192 (1971); D.R. Frankl, Electrical Properties of Semiconductor Surfaces, Pergamon Press, New York (1967); and A. Many, Y. Goldstein and R.B. Grover, Semiconductor Surfaces, North Holland, Amsterdam (1971)
6. C.B. Duke, A.R. Lubinsky, B.W. Lee and P. Mark, J.Vac.Sci.Technol. 13, 761 (1976) and references therein
7. G. Chiarotti, G. Del Signore and S. Nannarone, Phys.Rev.Lett. 21, 1170 (1968); G. Chiarotti, S. Nannorone, R. Pastore and P. Chiaradia, Phys.Rev. 134, 3398 (1971)
8. R. Ludeke and L. Esaki, Phys.Rev.Lett. 33, 653 (1974)
9. J. Rowe, Solid State Commun. 15, 1505 (1974)
10. W. Mönch, Advances in Solid State Physics, 13, 241 (1973)
11. G. Busch, T.E. Fischer, Physik Kondens. Materie 1, 367 (1963)
12. H.D. Hagstrum and T. Sakurai, Phys.Rev.Lett. 37, 615 (1976) and references therein
13. N.V. Smith, M.M. Traum and F.J. Di Salvo, Sol.State Commun. 15, 211 (1974)
14. N.V. Smith and M.M. Traum, Phys.Rev. B11, 2087 (1975)
15. P.J. Feibelman and D.E. Eastman, Phys.Rev. B10, 4932 (1974)
16. W. Gudat and C. Kunz, Phys.Rev.Lett. 29, 169 (1972)
17. G.J. Lapeyre, J. Anderson, P.L. Gobby and J.A. Knapp, Phys.Rev.Lett. 33, 1290 (1974)
18. D.E. Eastman and J.L. Freeouf, Phys.Rev.Lett. 33, 1601 (1974)
19. see e.g. chapter 15 of this book and references therein
20. G.M. Guichar, C.A. Sebenne and G.A. Garry, Phys.Rev.Lett. 37, 1158 (1976)

21. G.J. Lapeyre, A.D. Baer, J. Anderson, J.C. Hermanson, J.A. Knapp, and P.L. Gobby, Solid State Commun. 15, 1601 (1974)

22. J.J. Lander, G.W. Gobeli, and J. Morrison, J.Appl.Phys. 34, 2298 (1963)

23. M. Erbudak and T.E. Fischer, Phys.Rev.Lett. 29, 732 (1972)

24. J.V. Florio, W.D. Robertson, Surface Sci. 24, 173 (1971)

25. K.C. Pandey, T. Sakurai and H.D. Hagstrum, Phys.Rev.Lett. 35, 1728 (1975)

26. D. Haneman, Phys.Rev. 121, 1093 (1961); A. Taloni and D. Haneman, Surface Sci. 10, 215 (1968)

27. J.A. Appelbaum and D.R. Hamann, Phys.Rev. B12, 1410 (1975)

28. K.C. Pandey and J.C. Phillips, Phys.Rev.Lett. 34, 1450 (1975)

29. K.C. Pandey and J.C. Phillips, Phys.Rev. B13, 750 (1976)

30. F. Yndurain and L.M. Falicov, Solid State Commun. 17, 855 (1975)

31. E. Tosatti and P.W. Anderson, Solid State Commun. 14, 773 (1974)

32. A. Selloni and E. Tosatti, Solid State Commun. 17, 387 (1975)

33. S.G. Davison and J.D. Levine in Solid State Physics 25, 2 (1970) eds. H. Ehrenreich, F. Seitz, and D. Turnbull, Academic Press, New York

34. F. Garcia-Moliner and F. Flores, J.Phys. C: Solid State Phys. 9, 1609 (1976)

35. J.A. Appelbaum and D.R. Hamann, Rev.Mod.Phys. 48, 479 (1976)

36. J.A. Appelbaum and D.R. Hamann, Phys.Rev.Lett. 31, 106 (1973); ibid. 32, 225 (1974)

37. K.C. Pandey and J.C. Phillips, Phys.Rev.Lett. 32, 1433 (1974)

38. M. Schlüter, J.R. Chelikowsky, S.G. Louie and M.L. Cohen, Phys.Rev.Lett. 34, 1385 (1975)

39. M. Schlüter, J.R. Chelikowsky, S.G. Louie, and M.L. Cohen, Phys.Rev. B12, 4200 (1975)

40. M. Schlüter, J.R. Chelikowsky and M.L. Cohen, Phys.Lett. 53A, 217 (1975)

41. I.P. Batra and S. Ciraci, Phys.Rev.Lett. 34, 1337 (1975)

42. S. Ciraci and I.P. Batra, to be published

43. D.E. Eastman and W.D. Grobman, Phys.Rev.Lett. 28, 1378 (1972)

44. L.F. Wagner and W.E. Spicer, Phys.Rev.Lett. 28, 1381 (1972)

45. J.E. Rowe, Phys.Lett. 46A, 400 (1974)

46. J.E. Rowe, H. Ibach, and H. Froitzheim, Surface Sci. 48, 44 (1975)

47. L.F. Wagner and W.E. Spicer, Phys.Rev. B9, 1512 (1974)

48. T. Murotani, K. Fujiwara and M. Nishijima, Jap.J.Appl.Phys.Suppl. 22, 409 (1974)

49. J.E. Rowe, S.B. Christman and H. Ibach, Phys.Rev.Lett. 34, 874 (1975)

50. J.E. Rowe, M.M. Traum, and N.V. Smith, Phys.Rev.Lett. 33, 1333 (1973)

51. M.M. Traum, J.E. Rowe, and N.V. Smith, J.Vac.Sci.Technol. 12, 298 (1975)

52. J.E. Rowe and H. Ibach, Phys.Rev.Lett. 32, 421 (1974)

53. W.D. Grobman, D.E. Eastman and J.L. Freeouf, Phys.Rev. B12, 4405 (1975)

54. J.E. Rowe and H. Ibach, Phys.Rev.Lett. 31, 102 (1973)

55. B. Feuerbacher and R.F. Willis, J.Phys. C. Solid State Phys. 9, 169 (1976)

56. G. Chiarotti, P. Chiaradia, and S. Nanarone, Surface Sci. 49, 315 (1975)

57. J.A. Appelbaum, G.A. Baraff, and D.R. Hamann, Phys.Rev. B11, 3822 (1975); Phys.Rev.Lett. 35, 729 (1975)

58. R.E. Schlier and H.E. Farnsworth, J.Chem.Phys. 30, 917 (1959)

59. J.C. Phillips, Surface Sci. 40, 459 (1973)

60. P.M. Markus and D. Jepsen, private communication

61. J.E. Rowe and H. Ibach, Surface Sci. 43, 481 (1974)

62. T. Sakurai and H.D. Hagstrum, Phys.Rev. B14, 1593 (1976)

63. A. Koma and R. Ludeke, Phys.Rev.Lett. 35, 107 (1975); Surface Sci. 55, 735 (1976)

64. G. Margaritondo and J.E. Rowe, Phys.Lett. 59A, 464 (1977)

65. K. Hirabayashi, J.Phys.Soc. Japan 27, 1475 (1969)

66. D.J. Chadi and M.L. Cohen, Solid State Commun. 16, 691 (1975)

67. T. Murotani, K. Fujiwara and M. Nishijima, Phys.Rev. B12, 2424 (1975)

68. J.E. Rowe, Solid State Commun. 17, 673 (1975)

69. G. Chiarotti and S. Nannerone, Phys.Rev.Lett. 37, 934 (1976)

70. R. Ludeke and A. Koma, Phys.Rev.Lett. 34, 817 (1975)

71. R. Ludeke and A. Koma, Crit.Rev.Sol. State Sci. 5, 259 (1975)

72. J.L. Freeouf, Phys.Rev.Lett. 36, 1095 (1976)

73. A.V. MacRae and G.W. Gobeli, J.Appl.Phys. 35, 1629 (1964)

74. A.R. Lubinski, C.B. Duke, B.W. Lee, and P. Mark, Phys.Rev.Lett. 36, 1058 (1976)

75. J.R. Chelikowsky and M.L. Cohen, Phys.Rev. B13, 826 (1976)

76. K.C. Pandey, private communication and to be published

77. J.D. Joannopoulos and M.L. Cohen, Phys.Rev. B10, 5075 (1974)

78. P.E. Gregory, W.E. Spicer, S. Ciraci, and W.A. Harrison, Appl.Phys.Lett. 25, 511 (1974)

79. W.E. Spicer, P.W. Chye, P.E. Gregory, T. Sukegawa, and A. Babalola, J.Vac.Sci.Technol. 13, 233 (1976)

80. W.E. Spicer, I. Lindau, P.E. Gregori, C.M. Garner, P. Pianetta, and P.W. Chye, J.Vac.Sci.Technol. 13, 780 (1976)

81. C. Calandra and G. Santoro, J.Phys. C. Solid State Phys. 8, L86 (1975) and references therein

82. S.G. Louie, J.R. Chelikowski, and M.L. Cohen, J.Vac.Sci.Technol. 13, 790 (1976) and references therein

83. J.A. Knapp and G.J. Lapeyre, J.Vac.Sci.Technol. 13, 757 (1976)

84. R.A. Pollak, L. Ley, S. Kowalczyk, D.A. Shirley, J.D. Joannopoulos, D.J. Chadi, and M.L. Cohen, Phys.Rev.Lett. 29, 1103 (1972)

85. W. Gudat and D.E. Eastman, unpublished

86. W. Gudat and D.E. Eastman, J.Vac.Sci.Technol. 13, 831 (1976)

87. J.L. Freeouf and D.E. Eastman, Phys.Rev.Lett. 34, 1624 (1975)

88. J.L. Freeouf and D.E. Eastman, Crit.Rev.Sol. State Sci. 5, 245 (1975)

89. W. Gudat, E.E. Koch, P.Y. Yu, M. Cardona, and C.M. Penchina, phys.stat.sol. (b) 52, 505 (1972)

90. J.E. Rowe, S.B. Christman, and G. Margaritondo, Phys.Rev.Lett. 35, 1471 (1975)

91. A. Huijser and J. van Laar, Surf.Sci. 52, 202 (1975)

92. W. Gudat, D.E. Eastman and J.L. Freeouf, J.Vac.Sci.Technol. 13, 250 (1976)

93. J.C. Phillips, Phys.Rev.Lett. 22, 285 (1969)

94. G.J. Lapeyre and J. Anderson, Phys.Rev.Lett. 35, 117 (1975)

95. J.C. Phillips and K.C. Pandey, Surface Sci. 54, 183 (1976)

96. see e.g.,the various articles in J.Vac.Sci.Technol. 11 (1974) pp.935-991

97. J.O. McCaldin, T.C. McGill, and C. Mead, Phys.Rev.Lett. 36, 56 (1976)

98. J. van Laar and A. Huijser, J.Vac.Sci.Technol. 13, 769 (1976) and to be published

99. W. Ranke and K. Jacobi, Proc. of the 4th Int.Symp. Surface Physic, Eindhoven, June (1976) and to appear in Surface Science

100. W. Ranke and K. Jacobi, Solid State Commun. 13, 705 (1973)

101. K. Jacobi, Surface Sci. 51, 29 (1975)

102. D.J. Chadi and M.L. Cohen, Phys.Rev. B11, 732 (1975)

103. W.E. Spicer and P.E. Gregory, Crit.Rev. in Solid State Sci. 5, 231 (1975)

104. C. Calandra and G. Santoro, J.Vac.Sci.Technol. 13, 773 (1976)

105. R.S. Bauer, R.Z. Bachrach, S.A. Flodstrom, and J.C. McMenamin, J.Vac.Sci.Technol. 14,#1 (1977)

106. M. Henzler, Surface Sci. 25, 650 (1971)

107. G. Margaritando, J.E. Rowe and S.B. Christman, Phys.Rev. B14, 5396 (1976)

108. P. Pianetta, I. Lindau, C.M. Garner, and W.E. Spicer, Phys.Rev.Lett. 37, 1166 (1976)

109. P. Pianetta, I. Lindau, C. Garner, and W.E. Spicer, Phys.Rev.Lett. 35, 1356 (1975)

110. R. Dorn, H. Lüth, and G.J. Russell, Phys.Rev. B10, 5049 (1974)

111. W. Ranke and K. Jacobi, Surf.Sci. 47, 525 (1975)

112. M. Henzler, Surface Sci. 22, 12 (1970)

113. M. Henzler, Surface Sci. 36, 109 (1973)

114. V.T. Rajan and L.M. Falicov, J.Phys. C: Solid State Phys. 9, 2533 (1976)

115. M. Schlüter, K.M. Ho and M.L. Cohen, Phys.Rev. B14, 550 (1976)

116. T. Sakurai and H.D. Hagstrum, Phys.Rev. B12, 5349 (1975)

117. J.A. Appelbaum and D.R. Hamann, Phys.Rev.Lett. 34, 806 (1975)

118. K.C. Pandey, Phys.Rev. B14, 1557 (1976)

119. T. Sakurai and H.D. Hagstrum, J.Vac.Sci.Technol. 13, 807 (1976)

Figure captions

Fig. 11.1 Surface geometry of the ideal Si(111) surface (a) and of the Haneman model[26] for the Si(111)2x1 surface (b and c). Dangling bonds are indicated in the side view projections (d). Two-dimensional Brillouin zones corresponding to the ideal (111) (unreconstructed 1x1, dashed line) and the 2x1 reconstructed (heavy line) surfaces. Symmetry points are given according to Yndurain and Falicov[30] and Schlüter et al.[39] (in brackets). In references 27, 29 and 32 different notations are used.

Fig. 11.2 Local density of states (LDOS) of the first layer (surface atom layer) of a relaxed, unreconstructed Si(111) surface compared to the LDOS of the fourth layer and the density of states for the bulk. Spectral feature arising from the dangling bond and from relaxation induced surface states are indicated. (From Pandey and Phillips[29].)

Fig. 11.3 Density of states calculated from a 12 layer slab for the two dangling bond bands (d_{in} and d_{out}) of a reconstructed Si(111)-2x1 surface. The energy zero is taken at the bulk valence band edge. (From Schlüter et al.[39].)

Fig. 11.4 (a) Angle-integrated photoelectron energy distributions (cylindrical mirror analyser) for clean and contaminated Si(111)2x1 surfaces. The difference curve of the two spectra depicts the optical density of intrinsic surface states. (From Eastman and Grobman[43].) (b) Angular-resolved photoelectron spectra for a clean and contaminated cleaved Si(111) surface. Azimuthal angle ϕ=0 corresponds to the $[11\bar{2}]$. crystal direction. (After Rowe et al.[50].

Fig. 11.5 Angular-integrated photoemission spectra for three different Si surfaces: (a) (111)7x7, (b) (111)2x1 and (c) (100)2x1. The energy zero is taken at the bulk valence band maximum. Surface characteristic features A_1 to A_3 and B_1, B_2 are indicated for the (111)7x7 surface which are obtained as described in the text. (From Rowe et al.[52].)

Fig. 11.6 (a) Angular-integrated energy distributions for clean (curve a) and contaminated (curve b) 4 Ω-cm n-type cleaved Ge(111). The difference curve c denotes the optical density of intrinsic surface states. (After Eastman and Grobman[43].) (b) Partial yield spectra of clean (curve a) and Sb covered (curve b, ∿1 monolayer) n-type Ge(111) at the onset of transitions between 3d core states and empty surface states and conduction band states. A background due to valence band transitions has been subtracted in both spectra. The difference curve c denotes the empty surface state contribution. (After Eastman and Freeouf[18].)

Fig. 11.7 Surface geometry of the ideal (a) and fully relaxed (b) (bond angle $\eta = 35^{\circ}$) GaAs(110) surface. Dangling bonds are indicated in the sideview projections and the unit cell in the top-view. The two-dimensional Brillouin zone is shown in the extended zone scheme (c) Notation of critical points after Joannopoulus and Cohen.[77]

Fig. 11.8 Calculated local density of states (LDOS) of ideal and relaxed (bond angle change $\eta=35^{\circ}$) GaAs(110) using a SCF-pseudopotential method. Surface state features B_1' and B_1 to B_4 are indicated. The LDOS of layer 5 represents already that of the bulk. (From Louie et al.[82].)

Fig. 11.14 Various yield spectra for GaAs(110) are depicted all showing 3d core state- to -empty surface state transitions at 19.5 and 20.0 eV. (A) A partial yield spectrum normalized to the total photoyield of contaminated gold is shown with kinetic energy of the detected photoelectrons $E^* = 4$ eV. (B) A constant initial state spectrum is shown with the initial state $E_i = -6$ eV with respect to the valence band maximum. The CIS is normalized as described in (A). (C) A PYS at $E^* = 4$ eV is compared to the absorption edge[89] which does not show empty surface state transitions. In both spectra a background due to valence band transitions has been subtracted. (D) A total yield spectrum is shown together with its derivative spectrum. The spin orbit splitting of the 3d core states can be accurately determined ($\Delta_{so} = 0.45$ eV). Structures due to bulk critical points are seen above $h\nu = 20$ eV. Both spectra are not normalized, i.e. are somewhat distorted due to spectral intensity variations of the monochromator.

Fig. 11.15 Constant initial state spectra ($E_i = -1.2$) of GaAs(110) and ($\bar{1}\bar{1}0$) showing a dramatic dependence on the polarization of the light. Note the enhancement of the sharp surface state structure at 20 eV when the electric vector is parallel to the Ga derived dangling bonds. (After Lapeyre and Anderson[94].)

Fig. 11.16 Summary of one-electron empty-surface-state transition levels (E_s) for six III-V semiconductor surfaces (110). Here $E_s=h\nu_s - E_B(d_{5/2})$ is the one-electron transition-state energy measured relative to the valence-band maximum and does not contain excitonic corrections while E_F and E_o denote the Fermi level positions for the vacuum-semiconductor and Au-semiconductor interfaces (see text). The dashed lines schematically denote the bulk density of states and X_1,L_1 are bulk conduction band critical points.

Fig. 11.9 Calculated local density of states (LDOS) of ideal, partially relaxed (bond angle change η=19°) and fully relaxed (η=35°) GaAs(110) and DOS of bulk GaAs using the tight binding method. (After Pandey[76].)

Fig. 11.10 Angular resolved photoemission curves for a series of photon energies at fixed polar and azimuthal angles showing the emission of the surface state band B_1 at several values of $\underset{\sim}{k}_{//}$ (After Knapp and Lapeyre[83].) along the $\bar{\Gamma}$-$\bar{X}'$-$\bar{\Gamma}$ line in k-space.

Fig. 11.11 Experimentally determined[83] dispersion E_i versus $\underset{\sim}{k}_{//}$ of the surface state band B_1 of GaAs(110) along $\bar{\Gamma}$-$\bar{X}'$ direction compared to the dispersion curves calculated by Joannopoulus and Cohen[77] and by Pandey.[76]

Fig. 11.12 Angular resolved energy distributions of clean and H_2 exposed GaAs(110) showing emission attributed to the low lying surface state B_3. (After Knapp and Lapeyre[83].)

Fig. 11.13 Angle-integrated photoemission on the GaAs(110) surfaces at a photon energy hν = 30 eV shows contributions of surface states B_1 and B_3 in contrast to XPS measurements[84] at hν = 1486 eV. Surface state B_3 is indicated as determined from angular resolved photoemission (ARUPS)[83].

Fig. 11.17 Photoemission spectra at $\hbar\omega$ = 21.2 eV for the "dangling band" surface states near the valence band maximum E_{VB}. Cleavage step induced surface state structures (St) and intrinsic surface structures (2x1) are indicated. The observed surface potentials (E_F-E_V) are also given. The initial energy scale corresponds to curve b, and curves a and c have been shifted to align E_{VB}. (After Rowe et al.[49].)

Fig. 11.18 Calculated (dashed lines) and measured (heavy lines) UPS spectra are shown for clean Si(111)1x1 and for two chemisorption phases: a monohydride phase Si(111):H and a trihydride phase Si:SiH_3. The theoretical spectra are broadened by a Lorentzian of half width 0.3 eV. The ionization potential was taken to be 5.0 eV. (After Pandey et al.[25].)

Table I: Summary of band gaps, one-electron empty surface state transition energies (E_s) and Au-semiconductor interface Fermi levels (E_o), anion electronegativities[87] χ, estimated excitonic binding energies δ_{EX} and conduction band X_1 critical points for 6 (110) III-V semiconductors. All one-electron energies (in eV) are measured relative to the valence band maximum E_V.

	E_{gap}	X_1	E_s	E_o	χ	E_s-E_o	X_1-E_s	δ_{EX}
GaSb	0.70	∿1.8	0.65	0.15	1.9	0.5	1.15	>0.2
InSb	0.18	∿1.6	0.55	0.1		0.45	1.05	?
GaAs	1.43	1.9	0.9	0.5	2.0	0.4	1.0	>0.6
InAs	0.38	1.8	0.75	0.4		0.35	1.05	?
GaP	2.26	2.2	1.2	0.85	2.1	0.35	1.0	>0.6
InP	1.35	∿2.1	1.0	0.8		0.2	1.1	>0.4

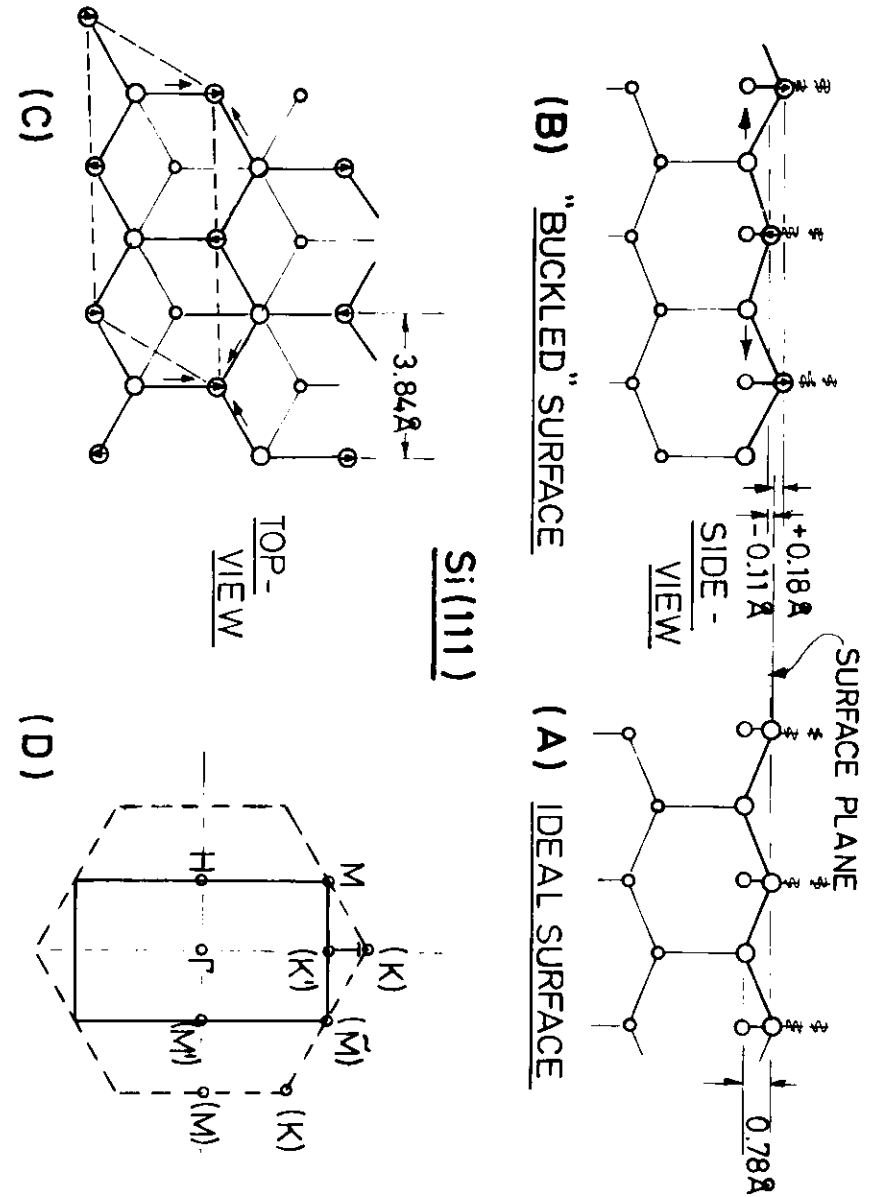

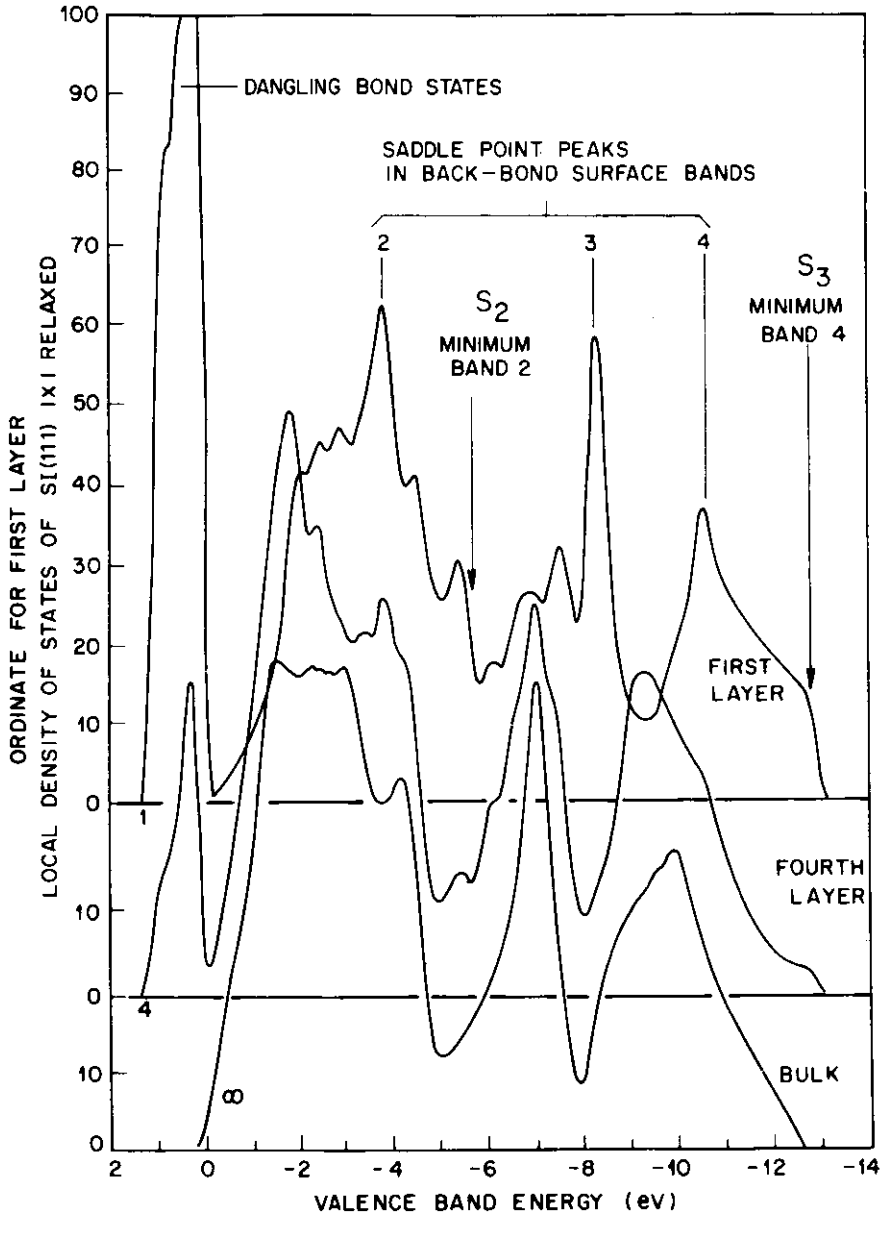
DANGLING BOND STATES
SADDLE POINT PEAKS
IN BACK-BOND SURFACE BANDS
2
3
4
S_2
MINIMUM
BAND 2
S_3
MINIMUM
BAND 4
FIRST
LAYER
FOURTH
LAYER
BULK
1
4
∞
ORDINATE FOR FIRST LAYER
LOCAL DENSITY OF STATES OF SI(111) 1X1 RELAXED
VALENCE BAND ENERGY (eV)

Fig. 2

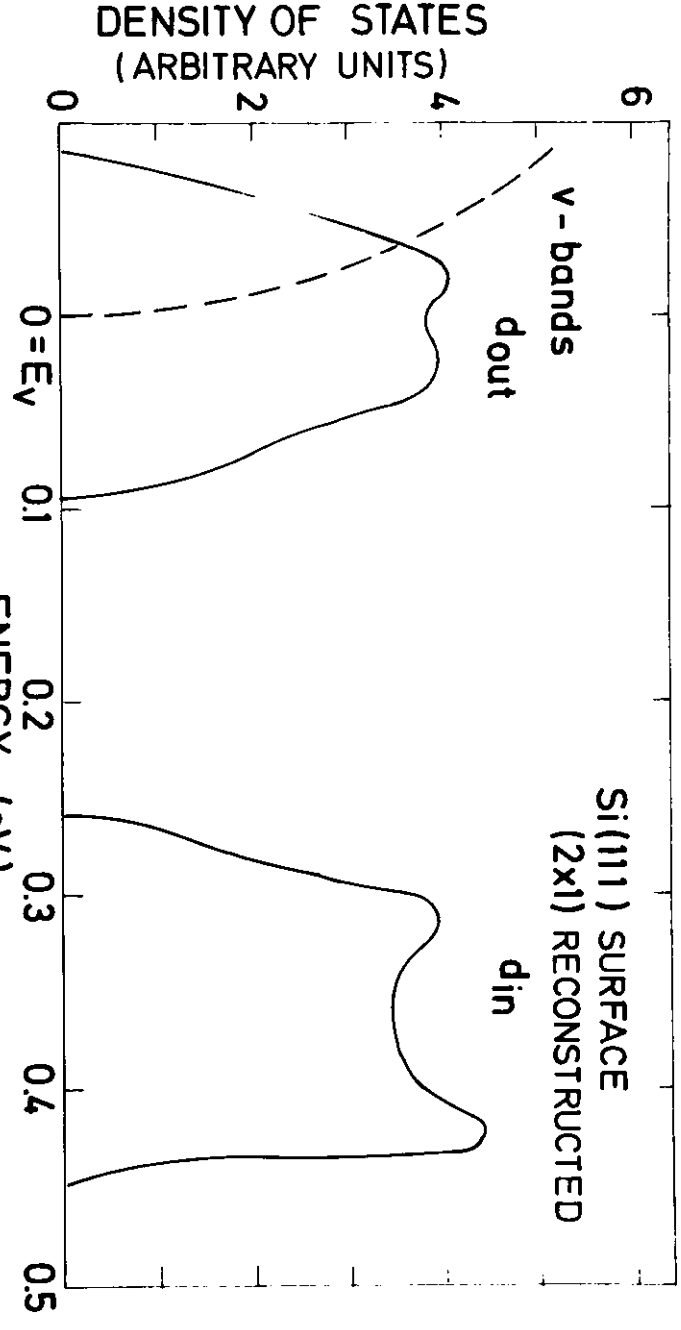
DENSITY OF STATES
(ARBITRARY UNITS)
v-bands
d_{out}
d_{in}
Si(111) SURFACE
(2x1) RECONSTRUCTED
$0 = E_v$
ENERGY (eV)

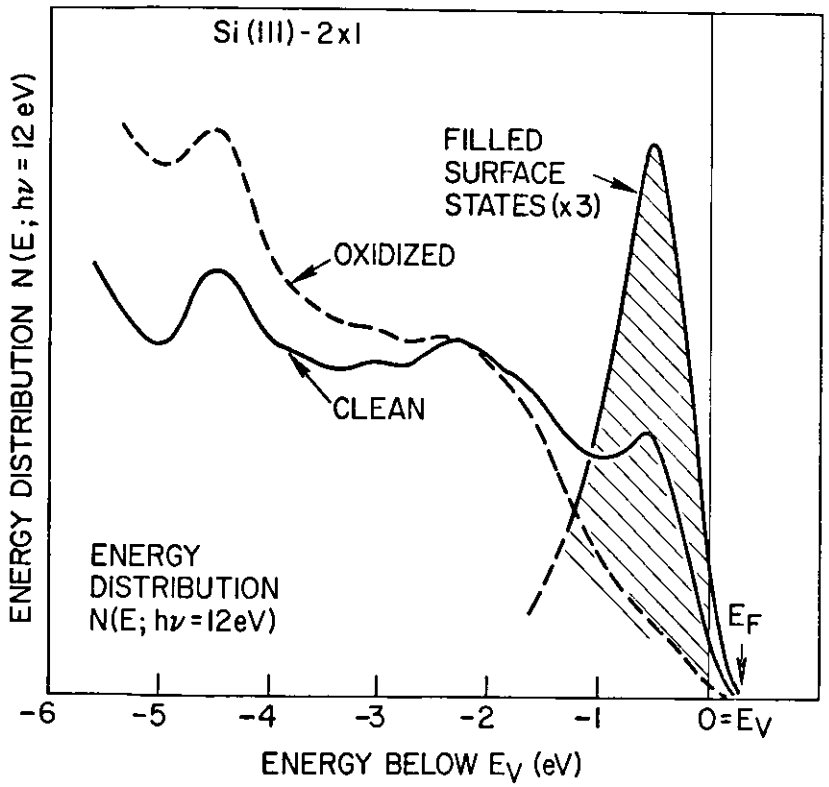

Fig. 4a

DESY

25999

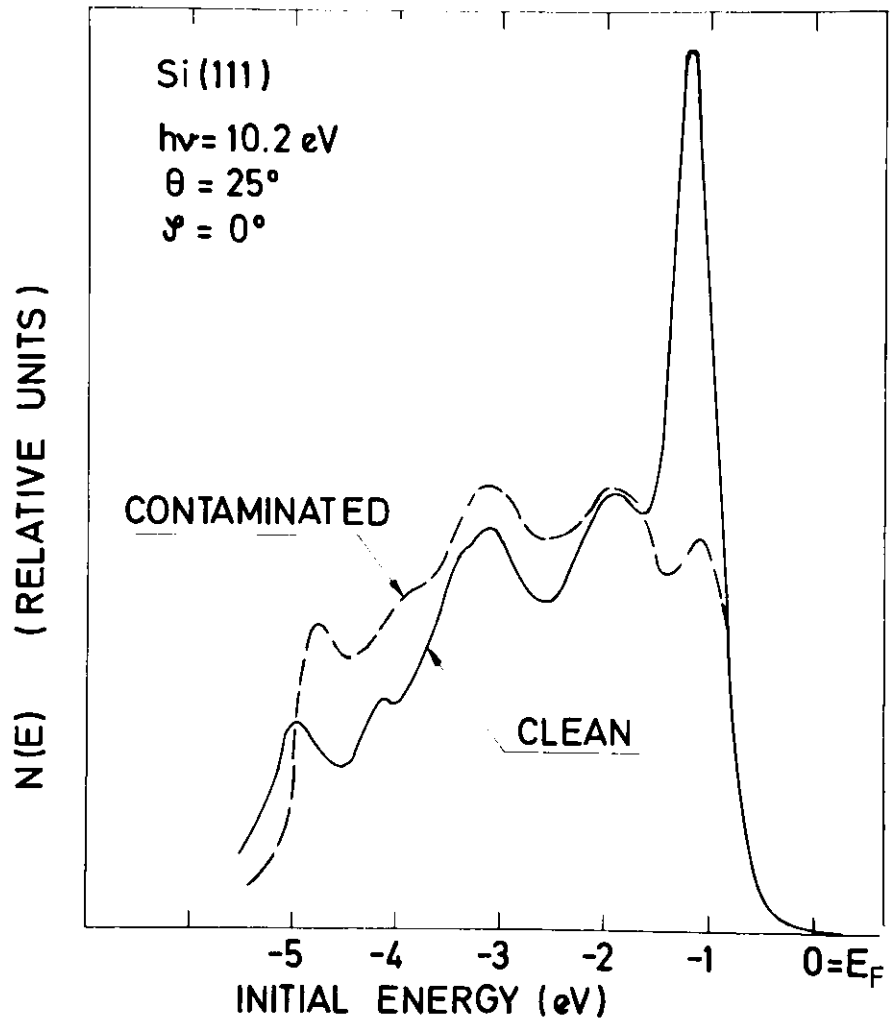

Fig. 4b

DESY
25952

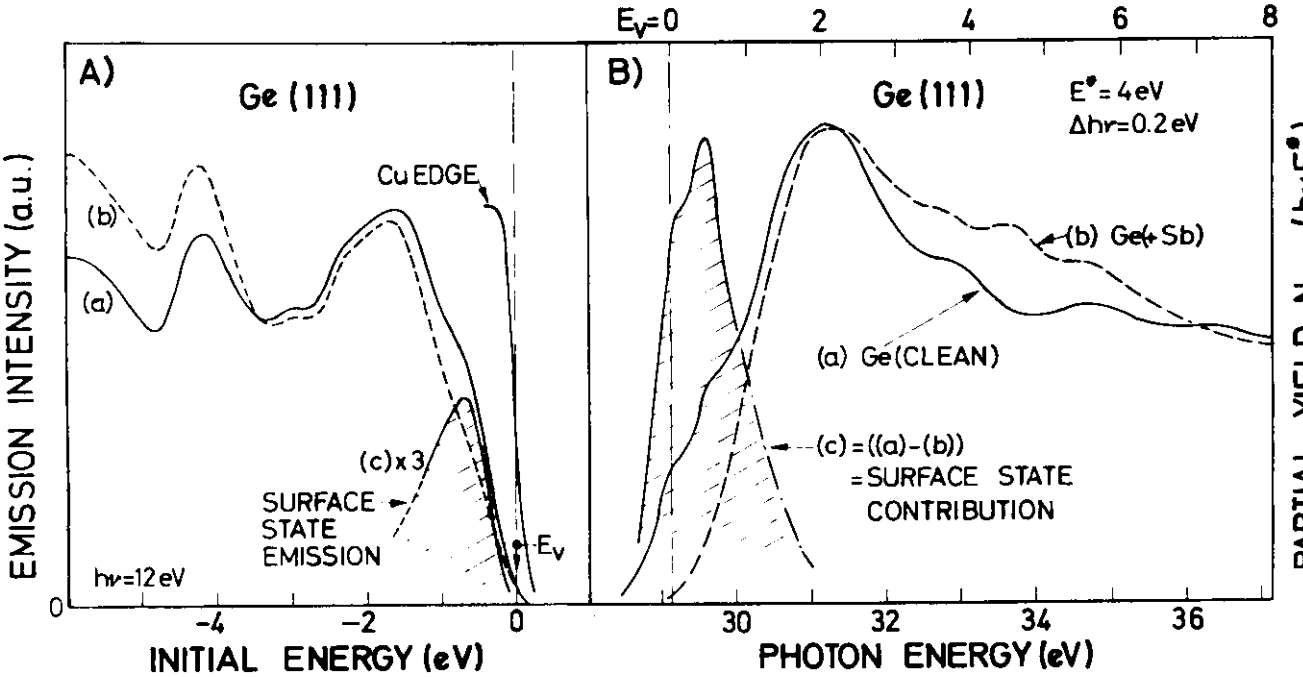

Fig. 4

DESY
25929

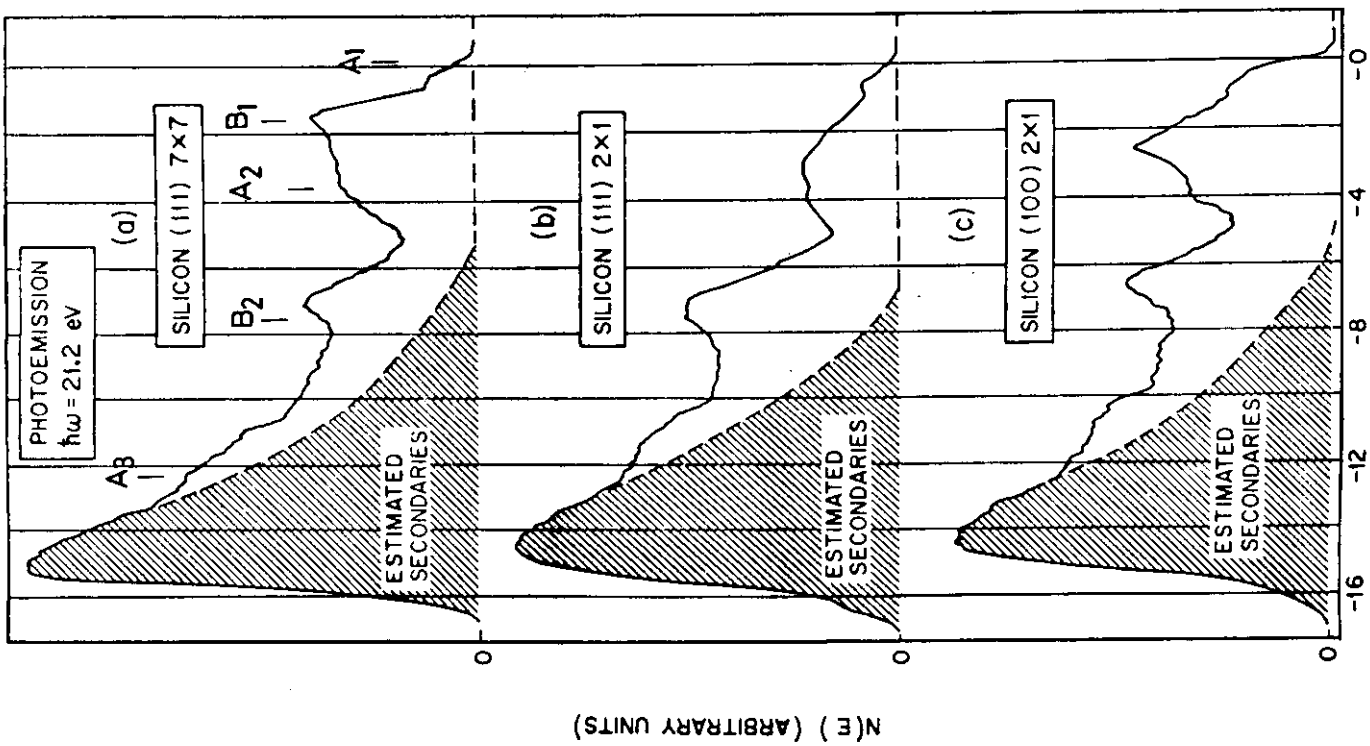

Fig. 5

26016
Ga As (110) SURFACE
LAYER 5
RELAXED
LAYER 1
IDEAL
LAYER 1
RELAXED
LAYER 2
RELAXED
B1
B1
B2
B3
B4
1.5
1.0
0.5
0
+2
0
-2
-4
-6
-8
-10
-12
ENERGY (eV)
LOCAL DENSITY OF STATES (ARBITRARY UNITS)

DESY
26017
η=35°
SIDE-
VIEW
As
Ga
SURFACE PLANE
GaAs (110)
IDEAL
RELAXED
UNIT CELL
TOP-
VIEW
(A)
(B)
(C)
M̄ (T̄10)
X̄
Γ̄
X̄
Γ̄
X̄'
M̄
(001)
Γ̄
Γ̄

Fig. 7

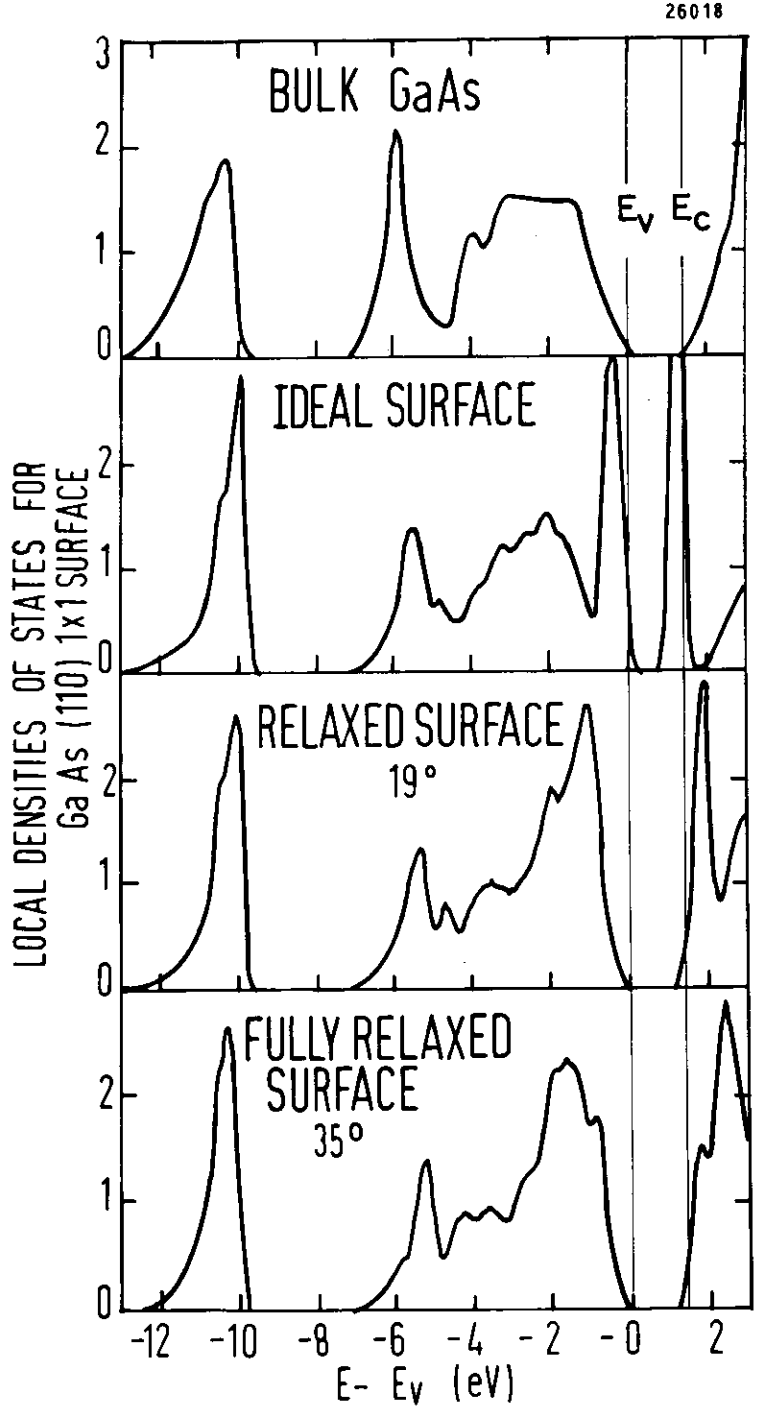
26018
BULK GaAs
E_v E_c
IDEAL SURFACE
RELAXED SURFACE
19°
FULLY RELAXED
SURFACE
35°
LOCAL DENSITIES OF STATES FOR
Ga As (110) 1x1 SURFACE
E- E_v (eV)

Fig. 9

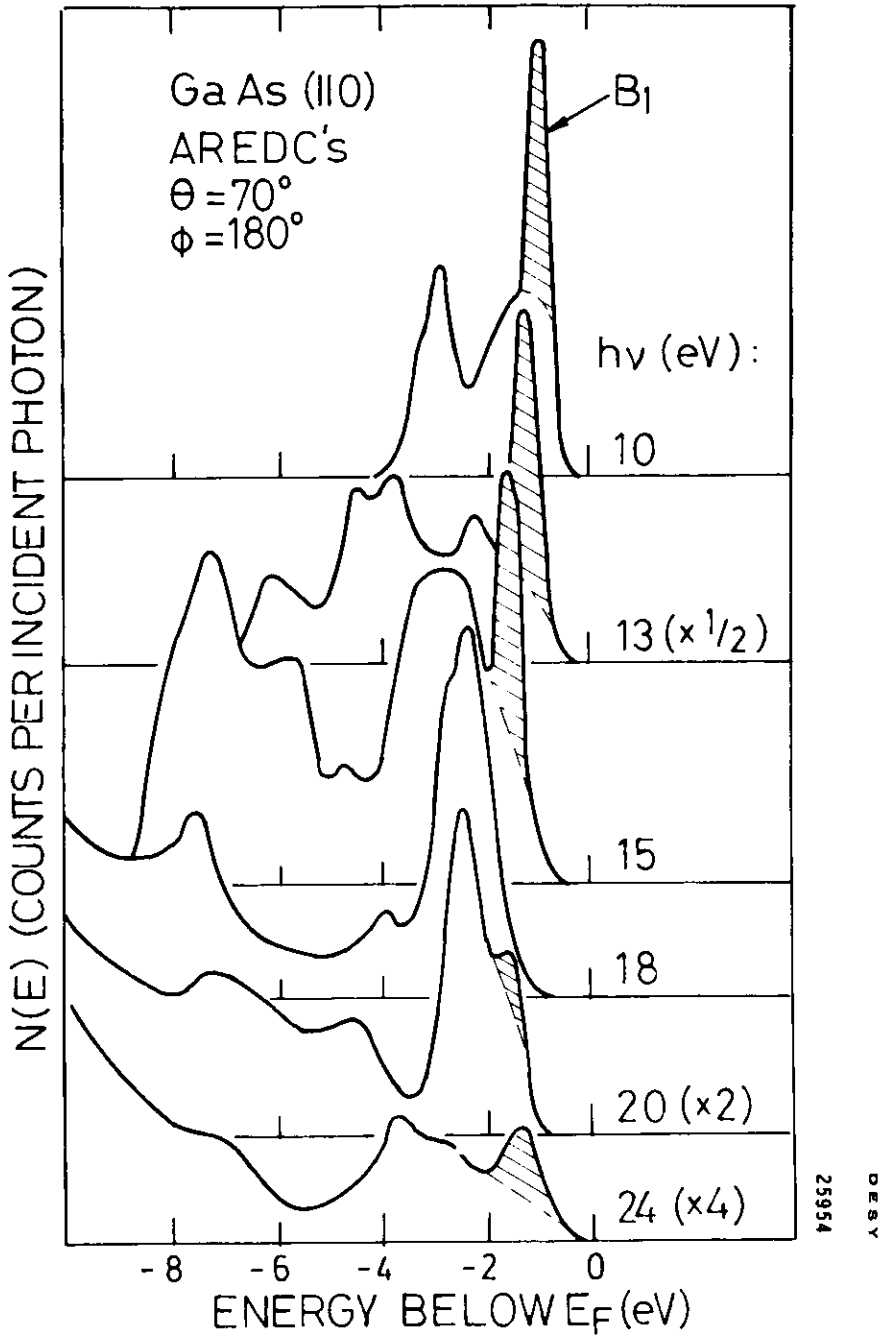
Ga As (110)
AREDC's
θ =70°
φ =180°
B_1
hν (eV):
10
13 (x 1/2)
15
18
20 (x2)
24 (x4)
N(E) (COUNTS PER INCIDENT PHOTON)
ENERGY BELOW E_F (eV)
25954
DESY

Fig. 10

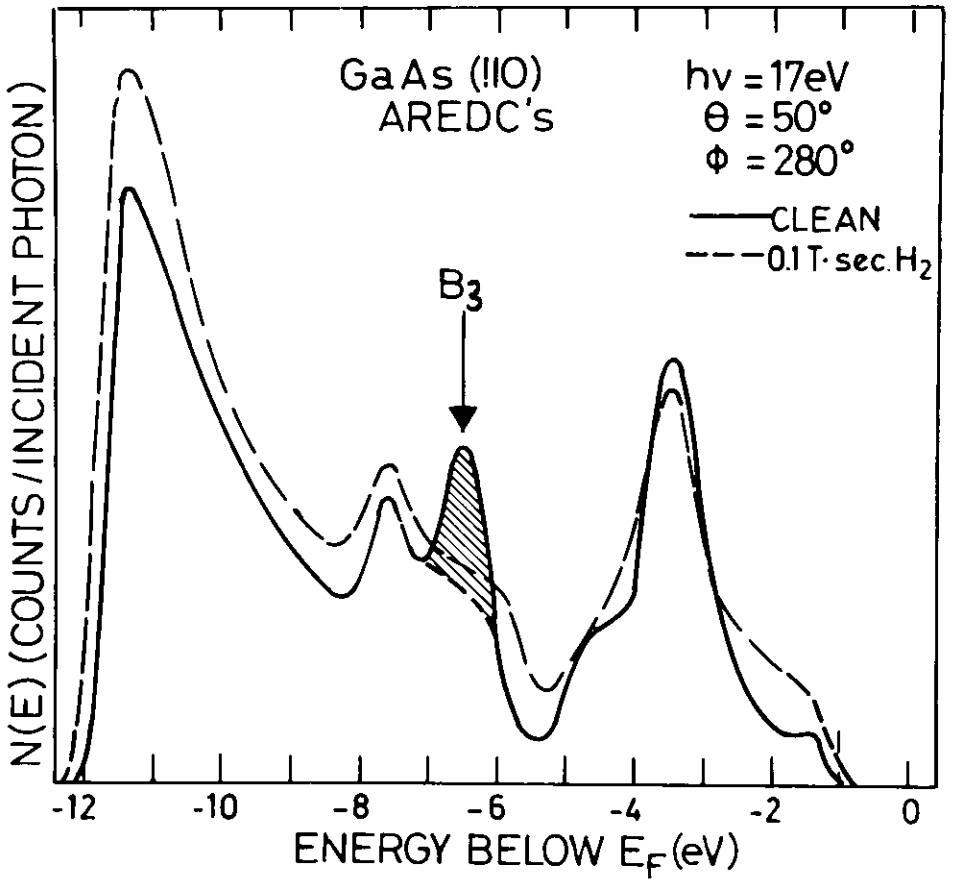
GaAs (110)
AREDC's
hν = 17eV
Θ = 50°
Φ = 280°
CLEAN
0.1 T·sec. H2
B3
N(E) (COUNTS / INCIDENT PHOTON)
-12
-10
-8
-6
-4
-2
0
ENERGY BELOW EF (eV)
25955
DESY

Fig. 12

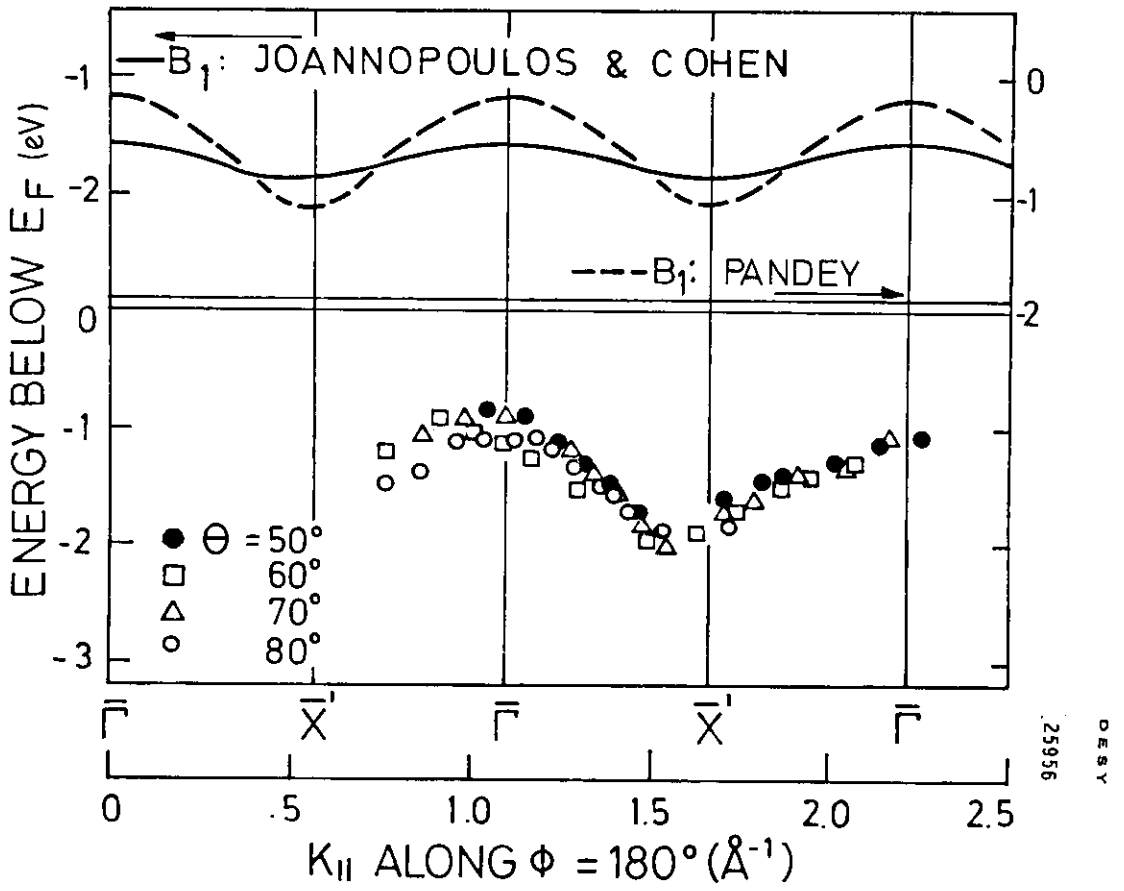
B1: JOANNOPOULOS & COHEN
B1: PANDEY
Θ = 50°
60°
70°
80°
ENERGY BELOW EF (eV)
-1
-2
0
-3
Γ̄
X̄'
Γ̄
X̄'
Γ̄
0
.5
1.0
1.5
2.0
2.5
K∥ ALONG Φ = 180° (Å-1)
25956
DESY

Fig. 11

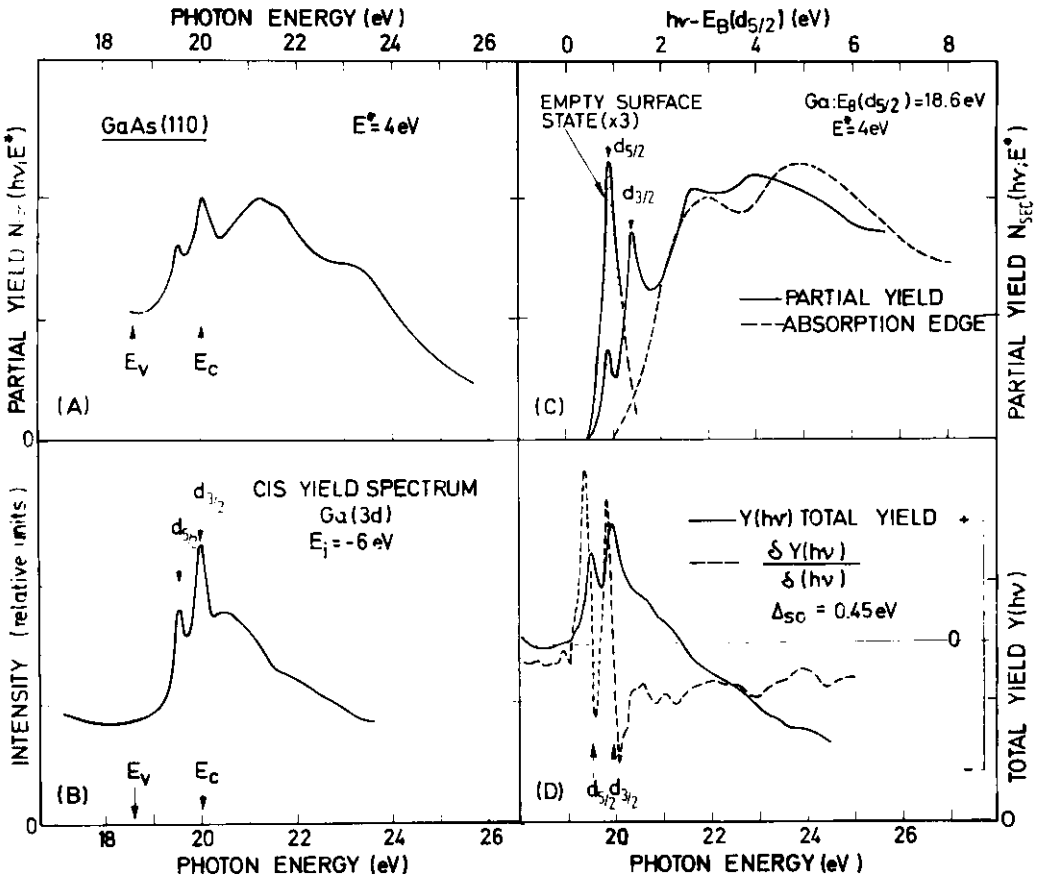
PHOTON ENERGY (eV)
hν-E_B(d_5/2) (eV)
GaAs(110)
E°=4eV
EMPTY SURFACE STATE(x3)
Ga:E_B(d_5/2)=18.6eV
E°=4eV
d_5/2
d_3/2
PARTIAL YIELD
ABSORPTION EDGE
PARTIAL YIELD N_tot(hν;E°)
PARTIAL YIELD N_sec(hν;E°)
(A)
(C)
E_v
E_c
CIS YIELD SPECTRUM
Ga(3d)
E_i=-6 eV
INTENSITY (relative units)
(B)
(D)
Y(hν) TOTAL YIELD
δ Y(hν) / δ(hν)
Δ_SO = 0.45eV
TOTAL YIELD Y(hν)
PHOTON ENERGY (eV)

Fig. 14

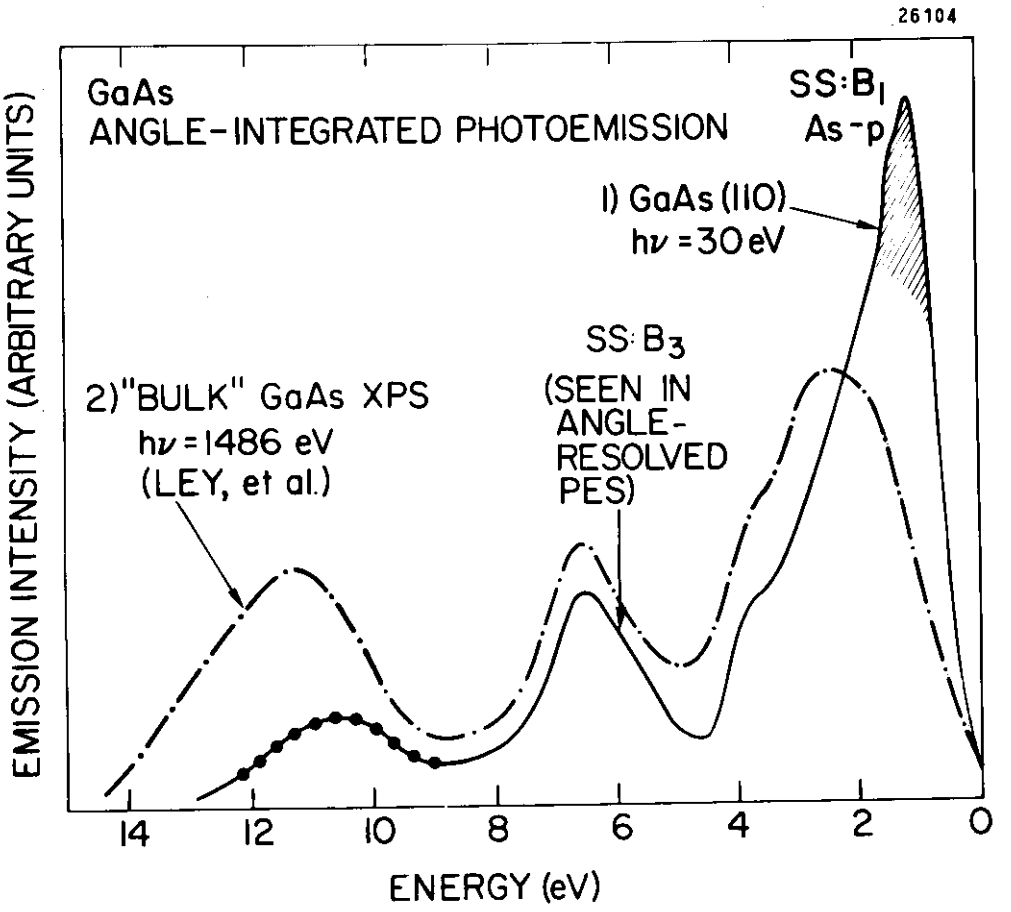
GaAs
ANGLE-INTEGRATED PHOTOEMISSION
SS:B1
As-p
1) GaAs (110)
hν = 30 eV
SS:B3
(SEEN IN ANGLE-RESOLVED PES)
2)"BULK" GaAs XPS
hν = 1486 eV
(LEY, et al.)
EMISSION INTENSITY (ARBITRARY UNITS)
ENERGY (eV)

Fig. 15

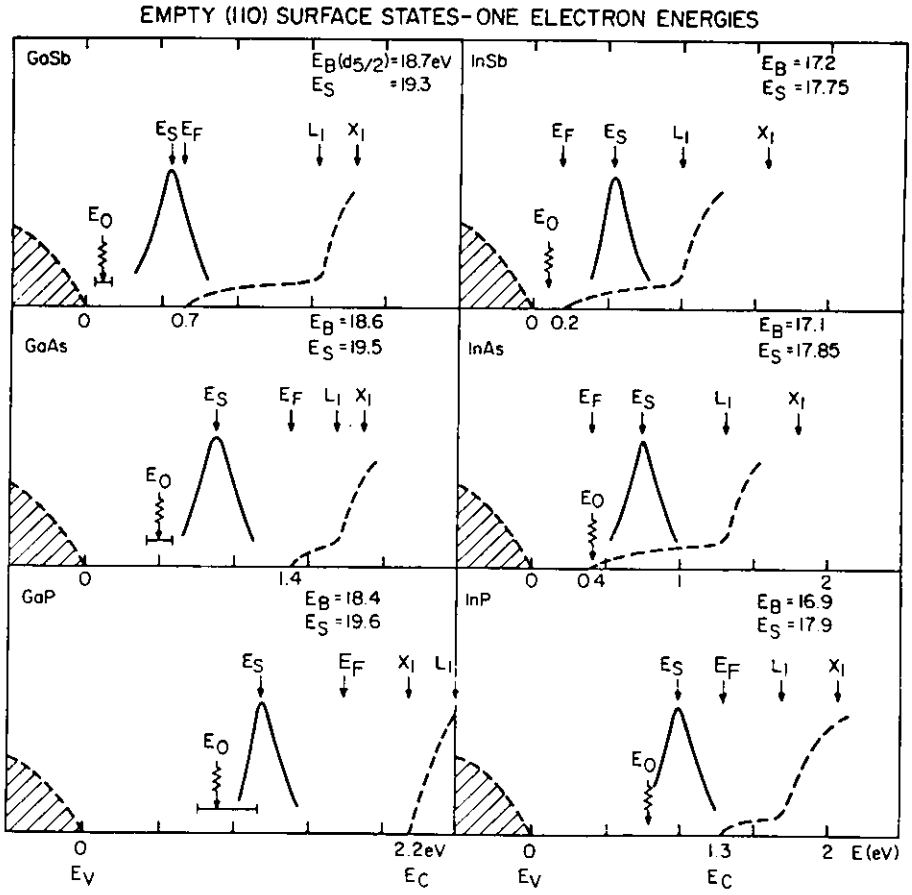
EMPTY (110) SURFACE STATES-ONE ELECTRON ENERGIES
GoSb
$E_B(d5/2)$=18.7eV
E_S =19.3
InSb
E_B =17.2
E_S =17.75
GaAs
E_B =18.6
E_S =19.5
InAs
E_B =17.1
E_S =17.85
GaP
E_B =18.4
E_S =19.6
InP
E_B =16.9
E_S =17.9
E_S
E_F
L_1
X_1
E_0
0
0.7
1.4
0.2
0.4
1
2
2.2eV
1.3
E(eV)
E_V
E_C

Fig. 16

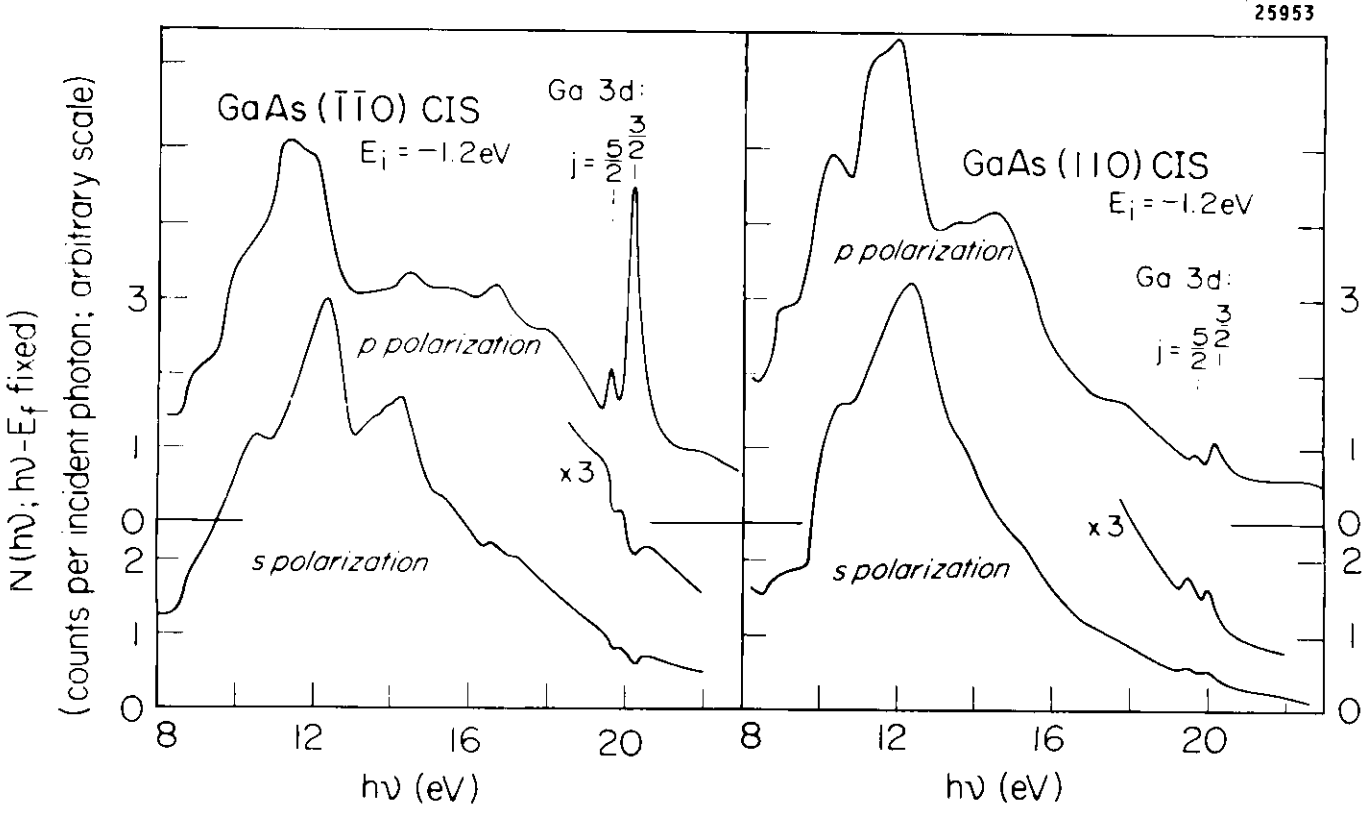
GaAs ($\bar{1}\bar{1}$0) CIS
E_i = −1.2eV
Ga 3d:
$j = \frac{5}{2}, \frac{3}{2}$
p polarization
s polarization
x 3
GaAs (110) CIS
E_i = −1.2eV
Ga 3d:
$j = \frac{5}{2}, \frac{3}{2}$
p polarization
s polarization
x 3
N(hν); hν-E_f fixed)
(counts per incident photon; arbitrary scale)
hν (eV)
hν (eV)
8
12
16
20
0
1
2
3

Fig. 15

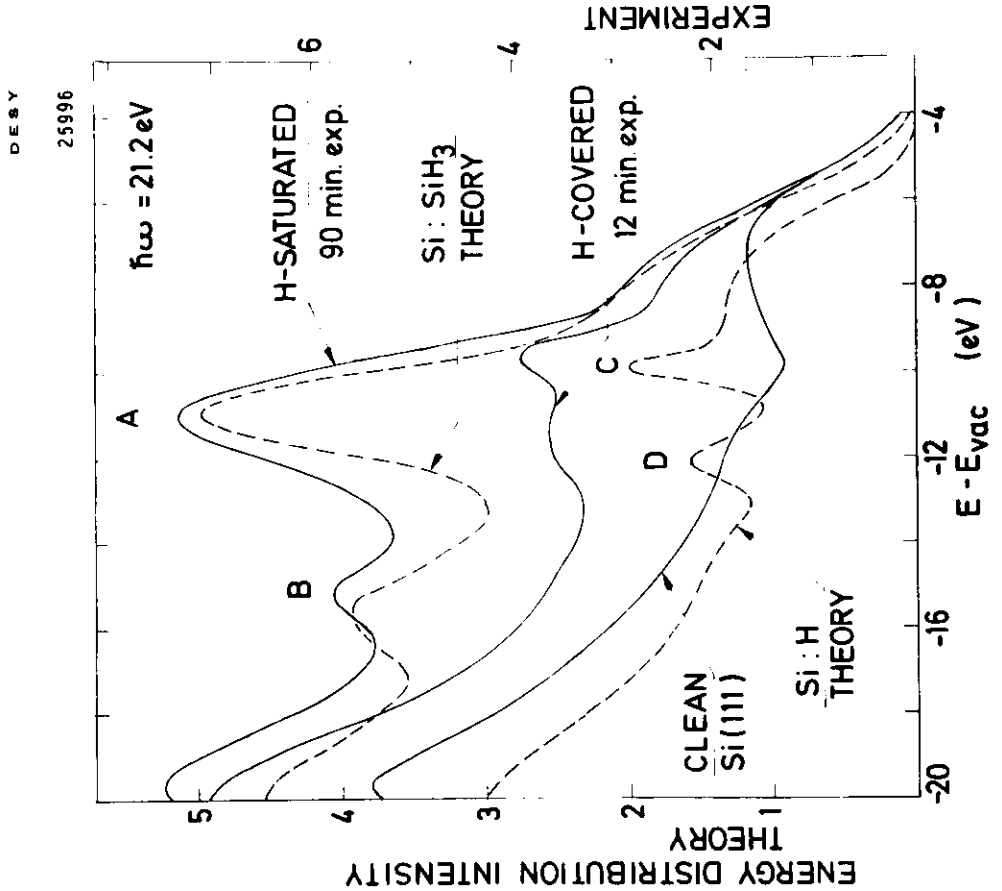
DESY
25996
ħω = 21.2eV
H-SATURATED
90 min. exp.
Si : SiH3
THEORY
H-COVERED
12 min. exp.
EXPERIMENT
A
B
C
D
CLEAN
Si(111)
Si : H
THEORY
E - Evac (eV)
ENERGY DISTRIBUTION INTENSITY
THEORY

Fig. 16

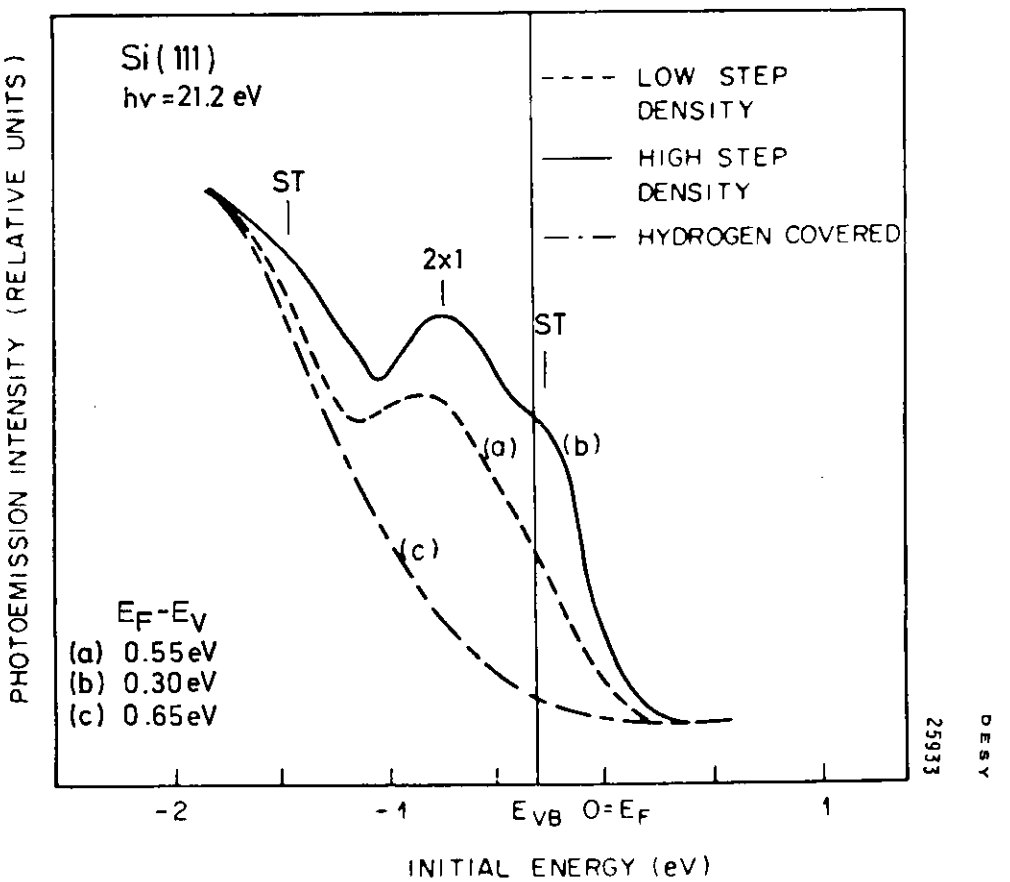
Si (111)
hν = 21.2 eV
LOW STEP DENSITY
HIGH STEP DENSITY
HYDROGEN COVERED
ST
2x1
ST
(a)
(b)
(c)
EF - EV
(a) 0.55eV
(b) 0.30eV
(c) 0.65eV
PHOTOEMISSION INTENSITY (RELATIVE UNITS)
EVB O=EF
INITIAL ENERGY (eV)
DESY
25933

Fig. 17